N73-18803

NASA TECHNICAL NOTE

NASA TN D-7188

NASA TN D-7188

CASE FILE COPY

ANALYTICAL AND EXPERIMENTAL PERFORMANCE OF OPTIMAL CONTROLLER DESIGNS FOR A SUPERSONIC INLET

by John R. Zeller, Bruce Lehtinen, Lucille C. Geyser, and Peter G. Batterton

Lewis Research Center
Cleveland, Ohio 44135

NATIONAL AERONAUTICS AND SPACE ADMINISTRATION • WASHINGTON, D. C. • MARCH 1973

1. Report No.	2. Government Accession No.	3. Recipient's Catalog No.
NASA TN D-7188		

4. Title and Subtitle	5. Report Date
ANALYTICAL AND EXPERIMENTAL PERFORMANCE OF OPTIMAL CONTROLLER DESIGNS FOR A SUPERSONIC INLET	March 1973
	6. Performing Organization Code
7. Author(s)	8. Performing Organization Report No.
John R. Zeller, Bruce Lehtinen, Lucille C. Geyser, and Peter G. Batterton	E-7173
	10. Work Unit No.
9. Performing Organization Name and Address	501-24
Lewis Research Center National Aeronautics and Space Administration Cleveland, Ohio 44135	11. Contract or Grant No.
	13. Type of Report and Period Covered
12. Sponsoring Agency Name and Address	Technical Note
National Aeronautics and Space Administration Washington, D.C. 20546	14. Sponsoring Agency Code

15. Supplementary Notes

16. Abstract

The techniques of modern optimal control theory were applied to the design of a control system for a supersonic inlet. The inlet control problem was approached as a linear stochastic optimal control problem using as the performance index the expected frequency of unstarts. The details of the formulation of the stochastic inlet control problem are presented. The computational procedures required to obtain optimal controller designs are discussed, and the analytically predicted performance of controllers designed for several different inlet conditions is tabulated. The experimental implementation of the optimal control laws is described, and the experimental results obtained in the Lewis 10- by 10-Foot Supersonic Wind Tunnel (SWT) are presented. The control laws were implemented with analog and digital computers. Comparisons are made between the experimental and analytically predicted performance results. Comparisons are also made between the results obtained with continuous analog computer controllers and discrete digital computer versions. Finally, recommendations of areas for further study are included.

17. Key Words (Suggested by Author(s))	18. Distribution Statement
Automatic control Optimal control Supersonic inlet	Unclassified - unlimited

19. Security Classif. (of this report)	20. Security Classif. (of this page)	21. No. of Pages	22. Price*
Unclassified	Unclassified	87	$3.00

* For sale by the National Technical Information Service, Springfield, Virginia 22151

CONTENTS

ANALYTICAL AND EXPERIMENTAL PERFORMANCE OF OPTIMAL CONTROLLER DESIGNS FOR A SUPERSONIC INLET

by John R. Zeller, Bruce Lehtinen, Lucille C. Geyser, and Peter G. Batterton

Lewis Research Center

SUMMARY

This report applies the techniques of modern optimal control theory to the design of a control system for a supersonic inlet. The inlet control problem was approached as a linear stochastic optimal control problem using as the performance index the expected frequency of unstarts. The details of the formulation of the stochastic inlet control problem are presented. The computational procedures required to obtain optimal controller designs are discussed, and the analytically predicted performance of controllers designed for several different inlet conditions is tabulated. The experimental implementation of the optimal controllers is described, and the experimental results obtained in the Lewis 10- by 10-Foot Supersonic Wind Tunnel (SWT) are presented.

The design studies showed that the amplitude-frequency distribution of the disturbance seen by the inlet has a large effect on the performance capabilities of the optimal controller. In this study two distinct disturbance spectra were assumed. The results show that the more disturbance energy there is at high frequency, the more difficult it is to control the inlet.

The experimental program pointed out certain of the problems involved in implementing a complex modern optimal controller. Controllers were implemented and evaluated with both analog and digital computer components. Analytically predicted and experimental frequency response performance compared quite well. The analog and digital computer implementations of a particular optimal controller design showed comparable performance results. Computer routines which were used to implement the digital computer version of an optimal controller are included. Recommendations as to further activities in using the capabilities of linear stochastic optimal control theory are also included.

INTRODUCTION

The techniques of modern optimal control theory have been applied to the design of a control system for a supersonic inlet. A supersonic inlet is that portion of a supersonic propulsion system which decelerates air from supersonic velocity (relative to the aircraft) ahead of the aircraft to subsonic velocity at the entrance to the compressor. This deceleration is needed because present compressors require subsonic air to operate efficiently. The dynamic head of supersonic air at high Mach numbers may comprise a large percentage of the overall propulsion system compression, and, therefore, efficient recovery of the pressure head is a critical part of the supersonic propulsion system. For subsonic propulsion systems, however, almost all the compression is done by the engine's compressor. To aid the supersonic inlet in operating at peak efficiency in the face of varying flight conditions, variable geometry features and associated controls are required.

A typical axisymmetric mixed compression inlet is shown in figure 1 in a normal operating configuration. Air at supersonic velocity enters the inlet past a weak oblique shock wave. It is compressed supersonically past a minimum area point, or throat, up to the terminal normal shock. Thereafter, the flow is subsonic up to the compressor face station.

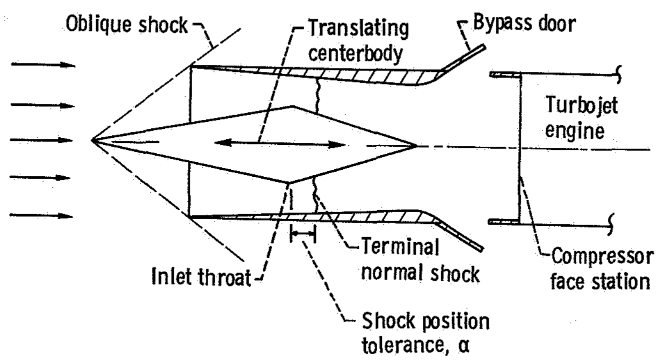

Figure 1. - Schematic of axisymmetric mixed compression supersonic inlet.

A stable operating condition for the inlet is one in which the throat Mach number is greater than one and the normal shock is downstream of the throat. This is the so-called started condition. An upstream or downstream disturbance may, however, cause the throat Mach number to drop to one, or it may cause the normal shock to move ahead of the throat. When either of these occur, the inlet unstarts and enters an undesirable, unstable operating region (called unstart).

During an unstart a shock wave sweeps out of the throat and a strong shock wave forms ahead of the inlet. The result is a large increase in drag and a large decrease in the pressure recovered at the compressor face. In addition, there may exist an oscillatory flow pattern within the inlet. Such a condition of unstart occurring in flight may not only interact with the engine, producing compressor stall and/or combustor flameout, but the increased nacelle drag and thrust loss can cause a sudden yawing of the aircraft. Control is required to maintain throat Mach number and terminal shock position within acceptable limits while maintaining efficient inlet operation.

Basic control devices are bypass doors and a variable centerbody. Opening the bypass doors allows air to be dumped overboard, causing the shock to move downstream away from the throat region. The movable centerbody varies the throat area, thereby varying the throat Mach number. A proper combination of these two control variables is used to ensure stable (started) inlet operation in the face of upstream and downstream disturbances.

Inlet control systems (refs. 1 and 2) have been designed to minimize system response to deterministic disturbances. Designs were obtained using frequency domain techniques. In reference 3, Barry conducted a design study based on an explicit description of inlet disturbances. The disturbance treated was atmospheric turbulence described by experimentally determined power spectral densities and probability distributions. The criterion used for evaluating inlet controls was the expected frequency of inlet unstart.

The control system to be discussed in this report has been designed to minimize the unstarts that would be initiated by a downstream (engine compressor face) airflow disturbance. This approach is an extension of the work of Barry. Initial work in this area has been presented in references 4 and 5. The inlet control problem was approached as a linear stochastic optimal control problem using, as the performance index, the expected frequency of unstarts. References 4 and 5 document the theoretical basis and computational procedures required in designing and analytically evaluating modern optimal inlet controllers.

The techniques of modern optimal control theory as applied to inlet control design are being investigated for several reasons. First, the modern approach provides a rigorous solution technique for optimizing a control design to some specific performance criterion. Second, the resulting control design will be stable. Stability is not necessarily assured when using conventional techniques. Third, the approach is general enough that system constraints can be included in the performance criterion. For example, in the inlet problem, limitations on bypass door position, velocity, and acceleration can be taken into account by a proper formulation of the criterion. Fourth, noisy measurements as well as random disturbances fit quite well into the modern optimal control formulation. Finally, the theory is such that it can handle the multiple-input - multiple-output control problem. The inlet control design, although it is not so considered in this report, can be expanded to a multiple input-output problem. Such an approach could sense additional pressures and pressure ratios throughout the inlet duct and control with centerbody as well as bypass doors.

The analytical inlet model used for the controls analysis of reference 4 was a simplified representation of an actual experimental variable geometry mixed compression supersonic inlet under evaluation at Lewis Research Center (refs. 6 to 8). Controller performance was evaluated analytically for wide spectrum (white) stochastic disturbances at two different levels of measurement noise on the sensed output variable. This report, however, expands the inlet model to include additional aspects such as (1) the response limitations of the actuators for the control input (overboard bypass doors) and (2) downstream airflow disturbances which have nonwhite (colored) power spectral densities. These considerations are required when the controller designs are to be implemented and evaluated experimentally on an inlet operating in a supersonic environment.

The rigorous solution techniques of modern optimal control design generate a controller configuration which in most cases is considerably more complex than one obtained by classical cut-and-try frequency domain techniques. It is the purpose of this report to discuss the procedures involved in determining the optimal design and then implementing with hardware the complex modern controller configuration. In addition, in determining the linear state-space inlet representation, several approximations to the real nonlinear distributed parameter inlet model have to be made. This report, therefore, uses results from the experimental operation of the controllers to determine the adequacy of these approximations.

The information is presented in two parts. First, the details of the formulation of the stochastic inlet control problem are discussed and documented. Along with this is a description of the computational procedures required to arrive at the optimal controller designs. Finally, a tabulation of the analytical results of controllers for several different inlet conditions is presented. In the second part, the details of the hardware implementations of controllers are described. This is followed by a presentation of the experimental results obtained in the Lewis 10- by 10-Foot Supersonic Wind Tunnel (SWT), as well as a comparison of these results with the frequency responses as predicted analytically. Finally, some recommendations are presented as to further efforts that would enhance this initial endeavor at applying optimal controller design to supersonic inlets.

CONTROLLER DESIGN AND ANALYTICAL PERFORMANCE

General Solution Technique

As stated earlier, the design techniques of modern optimal control theory have been applied to the design of a control system for a supersonic inlet. The purpose of the inlet control system considered here is to minimize the expected frequency of inlet unstarts to a random downstream airflow disturbance. Figure 2 is a block diagram of the general configuration chosen for this study.

As shown in figure 2, there are three distinct transfer functions, two defining the inlet and one the downstream (compressor face) disturbance. They are (1) the dynamics of the subsonic duct designated as $G_{INLET}(s)$, (2) the dynamics of the bypass doors to be used for control designated as $G_{BPD}(s)$, and (3) the transfer function $G_{NS}(s)$ (noise shaping network) which models the dynamics of the airflow disturbance to the duct. Each of these is discussed in detail in later sections of this report.

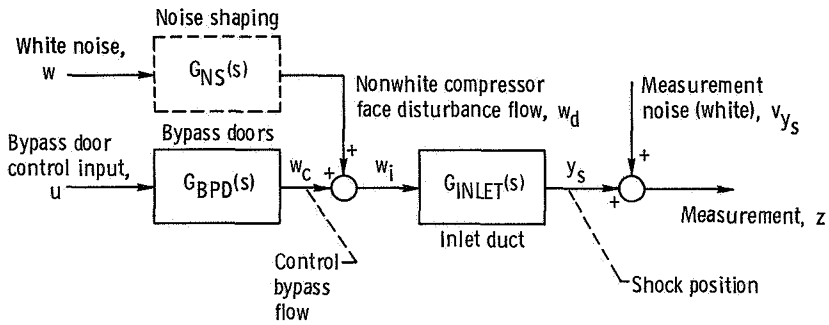

Figure 2. - Block diagram of typical inlet configuration.

The Gaussian compressor face disturbance w_d, shown in figure 2, is modeled as a white Gaussian airflow disturbance w being operated on by the transfer function $G_{NS}(s)$. The control input u operates the bypass doors and results in a corrective control airflow w_c. A measurement z of terminal normal shock position y_s is measured through a noisy channel with measurement noise v_{y_s}. The measurement noise is assumed to be white Gaussian.

For the inlet control design the following performance index was chosen to be minimized:

$$J = \lambda + k\sigma_u^2 \tag{1}$$

where

$$\lambda = \frac{1}{2\pi}\sqrt{\frac{\sigma_{\dot{y}_s}^2}{\sigma_{y_s}^2}}\exp\left(\frac{-\alpha^2}{2\sigma_{y_s}^2}\right) \tag{2}$$

and

λ expected frequency of inlet unstarts

k positive weighting factor

σ_u^2 mean-square value of control input

$\sigma_{\dot{y}_s}^2$ mean-square value of shock velocity

$\sigma_{y_s}^2$ mean square value of shock position

α shock position tolerance (distance between undisturbed shock position and inlet throat, see fig. 1)

The cost J was selected so that the control must minimize unstarts λ while limiting the amount of bypass door control effort σ_u^2 needed to do so. (All symbols are defined in appendix A.)

The λ relation (eq. (2)) gives the expected frequency with which the Gaussian random variable y_s exceeds the level α in the positive direction. The derivation of equation (2) can be found for instance in reference 9. The weighting factor k for σ_u^2 is selected to penalize the control variable so that the level of control effort will not exceed that which is available. (Selection of the control effort weighting factor k is discussed in a later section.) In order to use λ of equation (2) for this control design, the following assumptions must be made: (1) the inlet disturbances are Gaussian, (2) the inlet dynamics are linear, and (3) the controller is restricted to being linear and time invariant.

The approach taken in the designs being presented in this report uses the techniques of linear stochastic optimal control and estimation theory. This solution involves minimizing a quadratic type of performance index. It should be noted that the performance index of equation (1) is not quadratic because of λ. A linear optimal control law can, however, be determined by employing a technique termed the quadratic equivalence principle (ref. 10). This technique is used in this report. Since it has been previously described and used in reference 5, it is not repeated here. A summary of the type of control system which results is presented in the following section.

Linear Stochastic Optimal Control and Estimation Solution

A linear time invariant system can be described in state variable form as

$$\dot{x} = Ax + Bu + Dw \tag{3}$$

where x is an $n \times 1$ state vector, u is a $c \times 1$ control vector, and w is a $d \times 1$ plant disturbance vector. An $l \times 1$ output vector y is defined as

$$y = Cx \tag{4}$$

and an $m \times 1$ measurement vector is defined as

$$z = Hx + v \tag{5}$$

where v is an $m \times 1$ measurement noise vector. Both w and v are white zero mean Gaussian and uncorrelated with each other. Quantities A, B, C, D, and H are matrices of appropriate dimensions.

In solving the control and estimation problem (using the approach of ref. 11) for a quadratic performance index, the following equations result. The feedback control law is defined as

$$u = -K_c\hat{x} \tag{6}$$

where $\hat{x}$ is the optimal estimate of the state vector x and is generated with a Kalman filter described by

$$\dot{\hat{x}} = A\hat{x} + Bu + K_e(z - H\hat{x}) \tag{7}$$

The computation details for the constant matrices K_c and K_e are given in reference 4.

The block diagram in figure 3 illustrates the solution to the optimal control and estimation problem showing the state estimator and state estimator feedback. The state estimator (Kalman filter, eq. (7)) is basically a model of the plant driven by control u and measurement z. Signal z is compared with the estimated measurement $\hat{z}$ to form a term which is the error in the estimate of the measurement. This error is then multiplied by Kalman filter gains K_e and added back into the filter as a "correction" term. The filter output $\hat{x}$ is weighted by the control gains K_c to form the optimal control vector u. The portion of the system with measurement z as the input and control u as the output is defined as the optimal controller.

The following sections discuss the details of the design procedure as applied to the inlet problem.

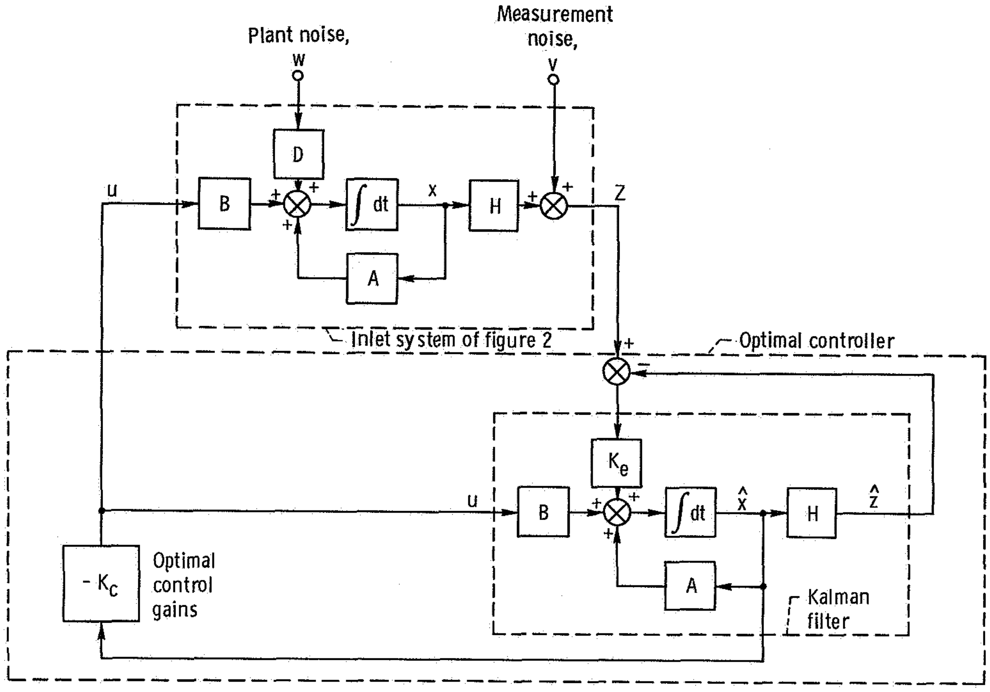

Figure 3. - Combined optimal regulator - state estimator.

Linear Continuous Time-Invariant Model Formulation

Inlet transfer functions. - The experimental mixed compression inlet, for which an optimal controller has been designed, has been the subject of evaluation in several past programs at Lewis Research Center. During these programs, the dynamic relations between a downstream (compressor face) disturbance and specific measurable variables throughout the inlet have been determined. These relations have been obtained through a frequency response testing method (refs. 6 and 8). In appendix B is a brief description of the method and how it was used in evaluating the inlet open loop frequency response performance. Appendix C contains the frequency response data obtained to describe the performance of the inlet. Also in appendix C is a complete tabulation of the transfer functions which have been curve fit to the experimental data. These transfer functions involve transportation lags or pure dead-time terms $\left(e^{-\tau_d s}\right)$. This is to be expected considering the distributed nature of the inlet duct. For comparison purposes, appendix C contains the frequency responses of the transfer function approximations to the experimental data.

For the inlet controls program being documented in this report, two specific measurements of shock location have been considered. One configuration uses a sensor which provides a stepwise continuous indication of actual inlet shock position. This type of sensing of the normal shock position has been accomplished in previous research programs (refs. 12 and 13). A brief description of the technique is also included in appendix B. The control using this measurement of actual shock position is designated as the shock position feedback or SPF system. It is described by the block diagram in figure 4. The second shock measurement configuration uses a static pressure downstream of the throat to indicate the position of the inlet normal shock. This is a more conventional way of obtaining an indication of shock position. For this second configuration, it was assumed that only the throat exit static pressure p_{te} was measurable for purposes of control. Thus, the inlet is uncontrolled or open loop to the actual shock position location. This configuration, which is shown in the block diagram in figure 5, shall be designated as the throat exit feedback or TEF system.

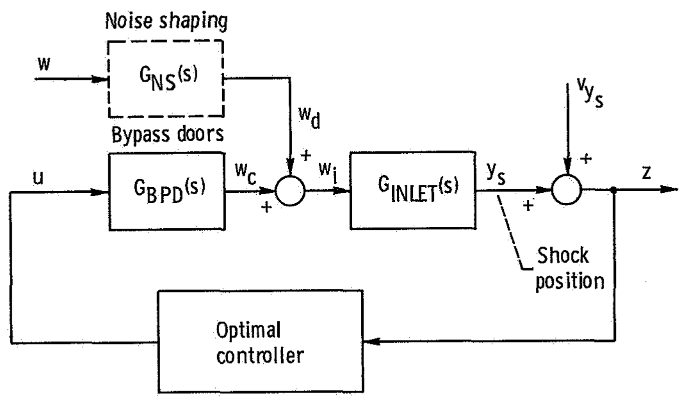

Figure 4. - Block diagram of shock position feedback (SPF) system of inlet control.

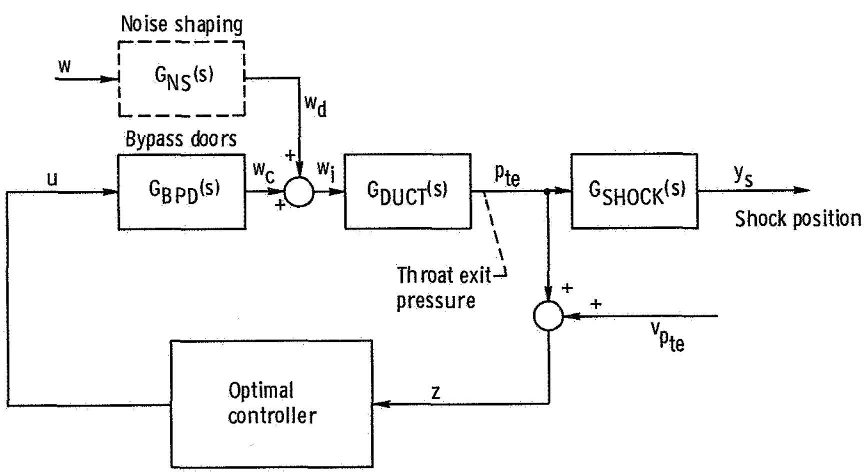

Figure 5. - Block diagram of throat exit feedback (TEF) system of inlet control.

For the SPF system (fig. 4), the transfer function relation of shock position y_s in response to a downstream (compressor face) airflow disturbance is given as

$$G_{INLET}(s) = \frac{y_s(s)}{w_i(s)} = \frac{16.25\left(\frac{s}{210} + 1\right)e^{-4.0\times10^{-3}s}}{\left(\frac{s}{80} + 1\right)\left(\frac{s^2}{365^2} + \frac{2(0.3)s}{365} + 1\right)} \quad \frac{cm}{kg/sec} \tag{C1}$$

Since our intent is to develop a finite-order state variable formulation of the inlet, the dead-time term of equation (C1), which has an infinite number of poles, must be modified. A finite-order approximation for the dead time was obtained using a Padé approximation. The transfer function for the SPF system inlet model can be written as

$$G_{INLET}(s) = \frac{y_s(s)}{w_i(s)}$$

$$= \frac{16.25\left(\frac{s}{210} + 1\right)\left(1 - 2\times10^{-3}s + 1.6\times10^{-6}s^2 - 0.533\times10^{-9}s^3\right)}{\left(\frac{s}{80} + 1\right)\left(\frac{s^2}{365^2} + \frac{0.6s}{365} + 1\right)\left(1 + 2\times10^{-3}s + 1.6\times10^{-6}s^2 + 0.533\times10^{-9}s^3\right)} \quad \frac{cm}{kg/sec} \tag{8}$$

using a third-order Padé.

For the TEF system (fig. 5), the two transfer functions are

$$G_{DUCT}(s) = \frac{p_{te}(s)}{w_i(s)} = \frac{1.52\left(\frac{s}{210} + 1\right)\left(\frac{s}{500} + 1\right)e^{-1.5\times10^{-3}s}}{\left(\frac{s}{80} + 1\right)\left(\frac{s^2}{365^2} + \frac{0.6s}{365} + 1\right)} \quad \frac{N/cm^2}{kg/sec} \tag{C2}$$

$$G_{SHOCK}(s) = \frac{y_s(s)}{p_{te}(s)} = \frac{10.68e^{-2.5\times10^{-3}s}}{\left(\frac{s}{500} + 1\right)} \quad \frac{cm}{N/cm^2} \tag{C3}$$

Again, as in the case of the SPF system, Padé approximations to the delay terms are used. Since the delay terms in equations (C2) and (C3) are both of shorter duration than the total duct delay of equation (C1), it was determined that first-order Padé approximations provided sufficient accuracy. The resulting transfer functions are

$$G_{DUCT}(s) = \frac{p_{te}(s)}{w_i(s)} = \frac{1.52\left(\frac{s}{210} + 1\right)\left(\frac{s}{500} + 1\right)(1 - 7.5\times10^{-4}s)}{\left(\frac{s}{80} + 1\right)\left(\frac{s^2}{365^2} + \frac{0.6s}{365} + 1\right)(1 + 7.5\times10^{-4}s)} \quad \frac{N/cm^2}{kg/sec} \tag{9}$$

$$G_{SHOCK}(s) = \frac{y_s(s)}{p_{te}(s)} = \frac{10.68(1 - 1.25\times10^{-3}s)}{\left(\frac{s}{500} + 1\right)(1 + 1.25\times10^{-3}s)} \quad \frac{cm}{N/cm^2} \tag{10}$$

Bypass door transfer function. - The mechanism used as the control input for the mixed-compression inlet under investigation are overboard bypass doors. These are fast-acting high-performance devices and are discussed in reference 14. Frequency response data from reference 14 are displayed in figure 6. As can be seen, the dynamics are not linear in that the performance varies as a function of the disturbance amplitude. Previous tests, however, have shown that a disturbance equivalent to the 14-percent level of door movement moves the shock position over a range quite adequate for

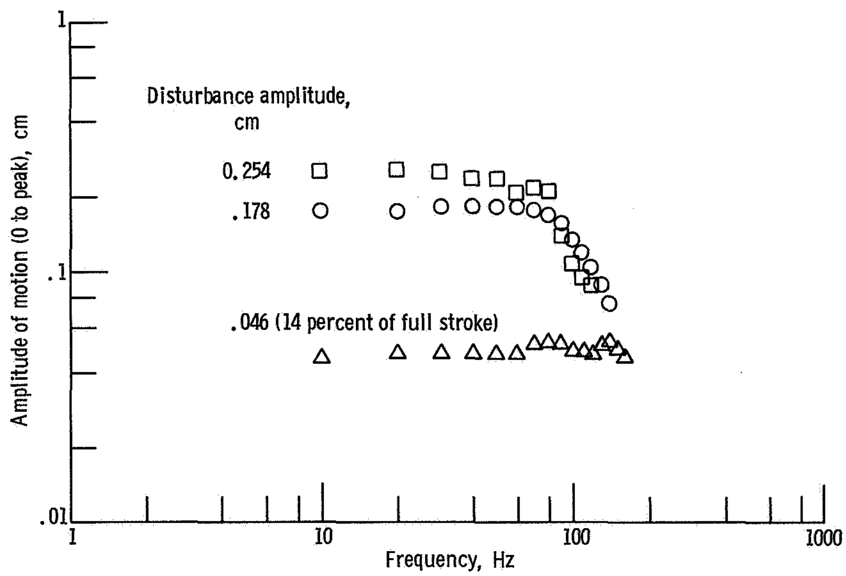

Figure 6. - Frequency response of inlet control bypass doors for three disturbance amplitudes.

investigation of inlet controller concepts. At this level of bypass airflow, the transfer function of equation (11) adequately describes the bypass door performance:

$$G_{BPD}(s) = \frac{w_c(s)}{u(s)} = \frac{0.9435}{\frac{s^2}{628^2} + \frac{2(0.5)s}{628} + 1} \quad \frac{\text{kg/sec}}{\text{V}} \tag{11}$$

Disturbance noise assumptions. - It has been pointed out earlier in this report that the inlet controllers were designed to minimize the expected frequency of unstarts to downstream disturbances. This is a statistical performance criteria and involves the mean-square value of shock position and shock velocity (ref. 4). Thus, a statistical description of the downstream disturbances is required. The linear stochastic optimal control theory formulation demands that the disturbance w be white Gaussian noise with zero mean. For the inlet problem, the disturbance w_d was not white. To model the spectrum of w_d, transfer functions were selected to shape a white noise input w. The presence of the required shaping transfer functions is shown by the dotted blocks in figures 4 and 5.

At the time of this program, no data were available to define the specific shape of the w_d spectrum. Therefore, two different disturbance spectra were assumed. Their asymptotic representations are shown in figure 7. The spectra were selected to allow

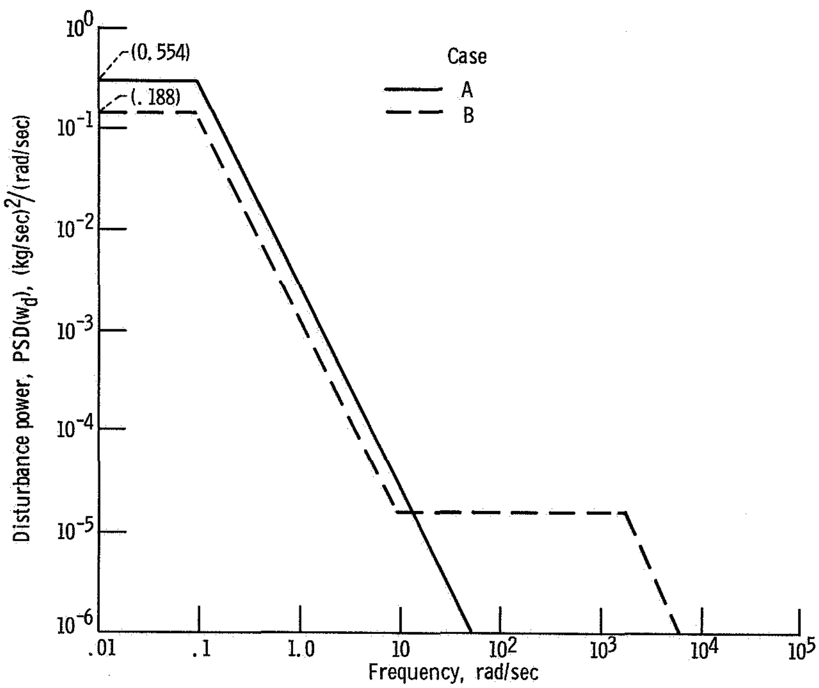

Figure 7. - Power spectral density of disturbance w_d (asymptotic representation).

the comparison of resulting optimal controller designs over as wide a range as seemed reasonable. To model the spectra shown in figure 7 as well as to allow for some flexibility in modeling other spectra in the future, the following generalized transfer function was used:

$$G_{NS}(s) = \frac{w_d(s)}{w(s)} = \frac{\left(\frac{s}{\alpha_2} + 1\right)}{\left(\frac{s^2}{\alpha_1\alpha_3} + \frac{(\alpha_1 + \alpha_3)}{\alpha_1\alpha_3} s + 1\right)} \tag{12}$$

For the spectra of cases A and B in figure 7, the α parameter values are shown in table I. To serve as a basis of comparison, it was decided that the mean-square value of the disturbance airflow would be the same regardless of the frequency spectrum selected. This was accomplished by modifying the power spectral density level of the white noise input w in accordance with the particular frequency spectrum selected. For the case A and case B spectra, the white noise input power spectral densities PSD(w) required to provide a constant mean-square airflow $\sigma_{w_d}^2$ equal to 0.0282 (kilogram per second)^2 are included in table I.

TABLE I. - FREQUENCY SPECTRUM PARAMETERS

FOR DISTURBANCE AIRFLOWS

Parameters	Case	
	A	B
Noise shaping transfer function parameters, rad/sec:		
α_1	0.1	0.1
α_2	5000	10
α_3	5000	2000
White noise input power spectral density, PSD(w), (kg/sec)^2/(rad/sec)	0.554	0.188
Mean-square value of disturbance airflow, $\sigma_{w_d}^2$, (kg/sec)^2	0.0282	0.0282

Measurement noise descriptions. - The signals of actual shock position y_s and throat exit static pressure p_{te} are used as the output measurements for the SPF and TEF systems, respectively. It has been assumed that these measurements are corrupted by specific levels of additive white Gaussian zero mean noise. This assumption is made at this time, since no spectral information of these measurement signals is available. In addition, as is discussed briefly in appendix B and in detail in reference 12, the shock position sensor generates a stepwise continuous representation of the location of the normal shock. No attempt has been made to include the quantization error of the sensor in the analysis. The noise levels assumed for this design study are

$$\mathrm{PSD}\left(v_{y_s}\right) = 3.22\times10^{-4}\ \mathrm{cm}^2\Big/\mathrm{rad/sec}$$

$$\mathrm{PSD}\left(v_{p_{te}}\right) = 2.38\ \left(\mathrm{N/cm}^2\right)^2\Big/\mathrm{rad/sec}$$

State Space Model Formulation

The transfer functions representing the inlet dynamics for the two configurations can now be formulated. The inlet frequency domain representations were transformed to the state variable form (eqs. (3) to (5)) by using the phase variable transformation (ref. 15). Tables II and III are the resulting numerical values for the matrices and and vectors for the SPF and TEF systems, respectively. The blocked-in sections come directly from the transfer functions indicated on the right. The nonblocked-in elements are the coupling between the transfer functions. The values of α_1, α_2, and α_3 for the case A and case B disturbance noise spectra are presented in table I.

It should be noted that both the SPF and TEF systems when put into the state space formulation are described by ten first-order differential equations (eq. (3)). Thus, the optimal inlet controller (eqs. (6) and (7)) consists of ten gains (K_e) defining a Kalman filter which generates ten state estimates ($\hat{x}$), which are weighted by ten feedback values (K_c).

With the state-space models of tables II and III the optimal controller design approach described earlier (documented in refs. 4 and 5) can now be undertaken. The computational details of this procedure are described in the next section.

TABLE II. - SHOCK POSITION FEEDBACK (SPF) SYSTEM STATE-SPACE MODEL MATRICES

A =	0	1									G_{INLET}
			1								
				1							
					1						
						1					
	-2.0012×10^{16}	-3.23×10^{14}	-1.158×10^{12}	-3.46×10^{9}	-4.8×10^{6}	-3.3×10^{3}	$\alpha_1 \alpha_3$	$\alpha_1 \alpha_3 / \alpha_2$	1		
							0	1			G_{NS}
							$-\alpha_1 \alpha_3$	$-(\alpha_1 + \alpha_3)$			
									0	1	G_{BPD}
	(a)								-3.95×10^{5}	-628	

B^T =	0	0	0	0	0	0	0	0	0	3.73×10^{5}

D^T =	0	0	0	0	0	0	0	1	0	0

C =	3.252×10^{17}	8.976×10^{14}	-2.576×10^{12}	2.303×10^{9}	-8.25×10^{5}	0	0	0	0	0

H =	3.252×10^{17}	8.976×10^{14}	-2.576×10^{12}	2.303×10^{9}	-8.25×10^{5}	0	0	0	0	0

[a]Blanks are all zeros.

TABLE III. - THROAT EXIT FEEDBACK (TEF) SYSTEM STATE-SPACE MODEL MATRICES

A =	0	1									G_{SHOCK}
	-4.0×10^5	-1.3×10^3	2.16×10^{10}	1.298×10^8	9.61×10^4	-1.542×10^2					
			0	1							G_{DUCT}
					1						
						1					
			-1.42×10^{10}	-2.12×10^8	-5.49×10^5	-1.632×10^3	$\alpha_1\alpha_3$	$\alpha_1\alpha_3\ \alpha_2$	1		
							0	1			G_{NS}
							$-\alpha_1\alpha_3$	$-(\alpha_1 + \alpha_3)$			
									0	1	G_{BPD}
	(a)								-3.95×10^5	-628	

B^T =	0	0	0	0	0	0	0	0	0	3.73×10^5
D^T =	0	0	0	0	0	0	0	1	0	0
C =	4.272×10^6	-5.34×10^3	0	0	0	0	0	0	0	0
H =	0	0	2.16×10^{10}	1.298×10^8	9.61×10^4	-1.542×10^2	0	0	0	0

[a]Blanks are all zeros.

Computational Design Procedures

It was desired that the optimal inlet controller be in the form of a combined controller-estimator as shown in figure 3. The design procedure is identical to that described in detail in reference 4. Therefore, the steps required to determine the estimator gains (K_e, eq. (7)) and optimal controller feedback gains (K_c, eq. (6)) are only summarized in this report. The estimator gains and the covariance matrix of the estimation error can be determined by solving an appropriate steady-state matrix Riccati equation using the inlet model and noise PSD's. To obtain the control gains K_c, a state regulator problem must be solved. The regulator has the task of minimizing the deviation of the appropriate states so as to accomplish the minimization of

$$J = \lambda + k\sigma_u^2 \tag{1}$$

when subjected to well defined compressor face airflow disturbances. As stated earlier, J involves the expected frequency of unstarts λ as well as the effort required to reduce the expected frequency of these unstarts. As was pointed out, λ is not a quadratic term. Thus, to use the results of linear stochastic optimal control theory and obtain a linear feedback solution, the quadratic equivalence principle is used. This principle is briefly outlined here.

Consider a general quadratic index in the variables of equation (1):

$$J_{eq}\left(\sigma_{\dot{y}_s}^2, \sigma_{y_s}^2, \sigma_u^2\right) = \left(\sigma_{\dot{y}_s}^2 + W_1\sigma_{y_s}^2 + W_2\sigma_u^2\right) \tag{13}$$

The differential of J_{eq} is simply

$$dJ_{eq} = d\sigma_{\dot{y}_s}^2 + W_1 d\sigma_{y_s}^2 + W_2 d\sigma_u^2 \tag{14a}$$

Similarly, the differential of J in equation (1) can be written as

$$dJ = \frac{\partial J}{\partial\sigma_{\dot{y}_s}^2}\left(d\sigma_{\dot{y}_s}^2 + \frac{\partial J/\partial\sigma_{y_s}^2}{\partial J/\partial\sigma_{\dot{y}_s}^2}\, d\sigma_{y_s}^2 + \frac{\partial J/\partial\sigma_u^2}{\partial J/\partial\sigma_{\dot{y}_s}^2}\, d\sigma_u^2\right) \tag{14b}$$

Now, assume a minimum of J_{eq} exists; thus,

$$dJ_{eq} = 0$$

Then, if

$$W_1 = \frac{\partial J/\partial\sigma_{y_s}^2}{\partial J/\partial\sigma_{\dot{y}_s}^2}$$

and

$$W_2 = \frac{\partial J/\partial\sigma_u^2}{\partial J/\partial\sigma_{\dot{y}_s}^2}$$

it can be seen by comparing equations (14a) and (14b) that $dJ = 0$, which indicates J has been minimized using the same gains K_c that minimized J_{eq}. Explicit conditions that must be satisfied for J to be minimized can be obtained from the aforementioned expressions for W_1 and W_2 by substituting for the required partial derivatives:

$$\left.\begin{aligned} W_1 &= \frac{\sigma_{\dot{y}_s}^2}{\sigma_{y_s}^2}\left(\frac{\alpha^2}{\sigma_{y_s}^2} - 1\right) \\ W_2 &= 4\pi k\sigma_{y_s}\sigma_{\dot{y}_s}\exp\left(\frac{\alpha^2}{2\sigma_{y_s}^2}\right) \end{aligned}\right\} \tag{15}$$

The computational technique for finding the minimum J is outlined in figure 8. There will be a minimum J for each value of the control weighting k. The procedure shown in figure 8 is repeated for each value of k.

To determine the minimum cost (J), trial pairs of W_1 and W_2 (designated as W_1^* and W_2^*) are used as inputs to the optimal regulator portion of the solution. The feedback gains K_c are determined by solving a steady-state matrix Riccati equation. Using these gains and the covariance matrix of the estimation error, the steady-state state-covariance matrix equation is solved to determine mean-square values of the states.

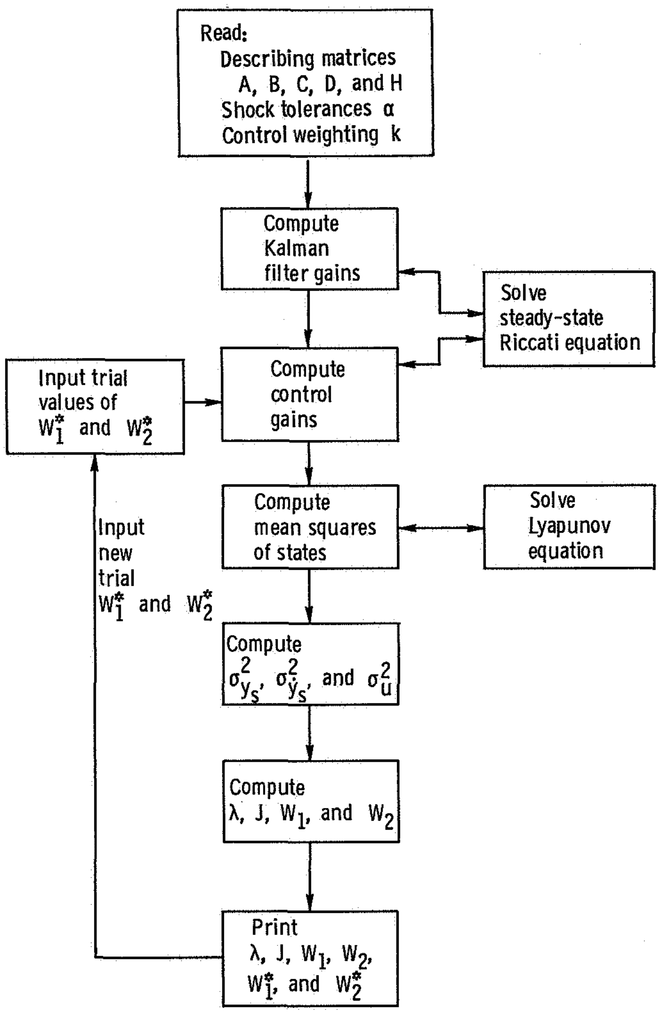

Figure 8. - Computation procedure flow chart.

(This involves solving a Lyapunov equation.) The mean-square state information is used to determine $\sigma_{y_s}^2$, $\sigma_{\dot{y}_s}^2$, and σ_u^2 values. These are used to compute J and λ as well as W_1 and W_2. When the values of W_1 and W_2 computed by equations (15) are equal to the trial W_1^* and W_2^* values, then equivalence is achieved and the cost J is at a minimum value for that value of control weighting k.

A search routine on W_1^* and W_2^* could have been used to find the minimum cost. However, it was decided that selected pairs of W_1^* and W_2^* be used, which would encompass the field of possible values, and that both the optimum and nonoptimum solutions would be printed. This list was then searched manually to find the optimum solutions. The search was done to see the full deviations of the nonoptimum solutions from the optimum.

Analytical Design Results and Discussion

A family of optimal controllers has been designed for each of the four systems discussed earlier. These controllers are as follows:

(1) SPF system, case A disturbance

(2) TEF system, case A disturbance

(3) SPF system, case B disturbance

(4) TEF system, case B disturbance

Analytical results of the design procedure are presented and discussed in this section.

If the inlet were left open loop and the undisturbed steady-state position of the shock (α) set by a fixed bypass door opening, then the unstart performance shown in figure 9 would result. Note that the ordinate is the inverse of the frequency of unstarts. The mean time between unstarts λ^{-1} in hours should be a more understandable numerical quantity for the reader.

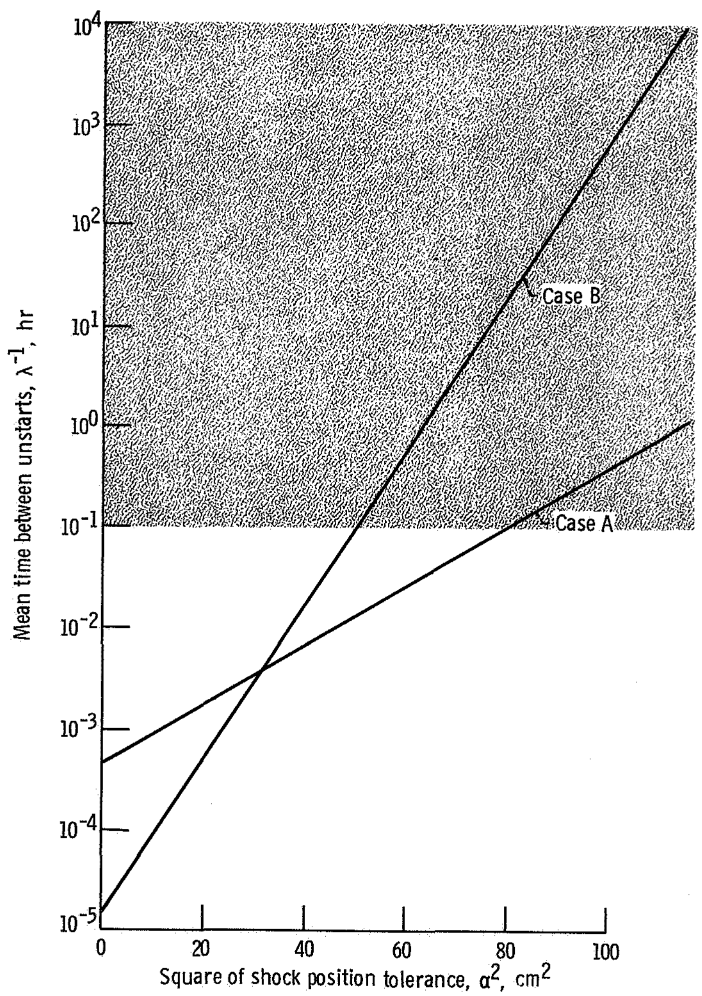

Figure 9. - Open loop (no control) unstart performance.

Figure 9 is a log-linear plot of λ^{-1} against α^2 for both case A and case B disturbances. It should be remembered that $\sigma^2_{w_d}$ is the same for both cases. The straight lines are due to log (λ^{-1}) being a linear function of α^2. This can be seen by examining the equation which defines λ (eq. (2)). The $\alpha = 0$ intercepts for the lines are given by (see eq. (2))

$$2\pi\sqrt{\sigma^2_{y_s}\Big/\sigma^2_{\dot{y}_s}}$$

This is the inverse of what is termed the "zero crossing frequency." This intercept is smaller for case B than for case A because of the relative magnitudes of $\sigma^2_{y_s}$ and $\sigma^2_{\dot{y}_s}$. The slope of a line is $\left(2\sigma^2_{y_s}\right)^{-1}$. This quantity is smaller for case A; thus, mean time between unstarts for case A is less sensitive to α than in case B. The reason $\left(2\sigma^2_{y_s}\right)^{-1}$ is smaller for case A is that in case A most of the energy is concentrated at low frequencies where the disturbance energy is not greatly attenuated by the inlet duct. Conversely, for case B, more disturbance energy is present at high frequencies where the inlet attenuation is large; hence, the resulting mean-square shock position is less than for case A.

Figures 10 to 13 represent the inlet unstart performance for each of the inlet problems being evaluated. On each of these figures the ordinate is the time between unstarts λ^{-1} and covers the same range as that of the shaded area of the open-loop performance shown in figure 9.

The abscissa for these four figures is σ_u, the rms control effort in volts. This factor was part of the performance index of equation (1). Each value of σ_u corresponds to a different value of control weighting k and thus a different set of feedback gains K_c. In looking at the curves for any fixed value of shock setting α, the time between unstarts increases as the amount of control effort σ_u increases. Also, for a fixed control effort but an increased α, λ^{-1} is greater.

In figure 10 for SPF case A there is a sharp increase in λ^{-1} in the area of σ_u = 0.175 volt. Beyond 0.20 volt, no significant gain in performance can be accomplished. This type of control performance is also seen in figure 11 for TEF case A which is the same disturbance case. When comparing figures 10 and 11 it can be seen that SPF system can use lower α settings to accomplish the same unstart performance. Thus, for the case A disturbance, control can better be accomplished by directly sensing the output y_s even though an additional measurement lag is incurred in doing so. This is due to the relatively high measurement noise level present on the p_{te} measurement signal.

Also shown in figure 10 is a notation which indicates the shock setting that would be required for an open-loop system to yield 100 hours between unstart. At this setting of

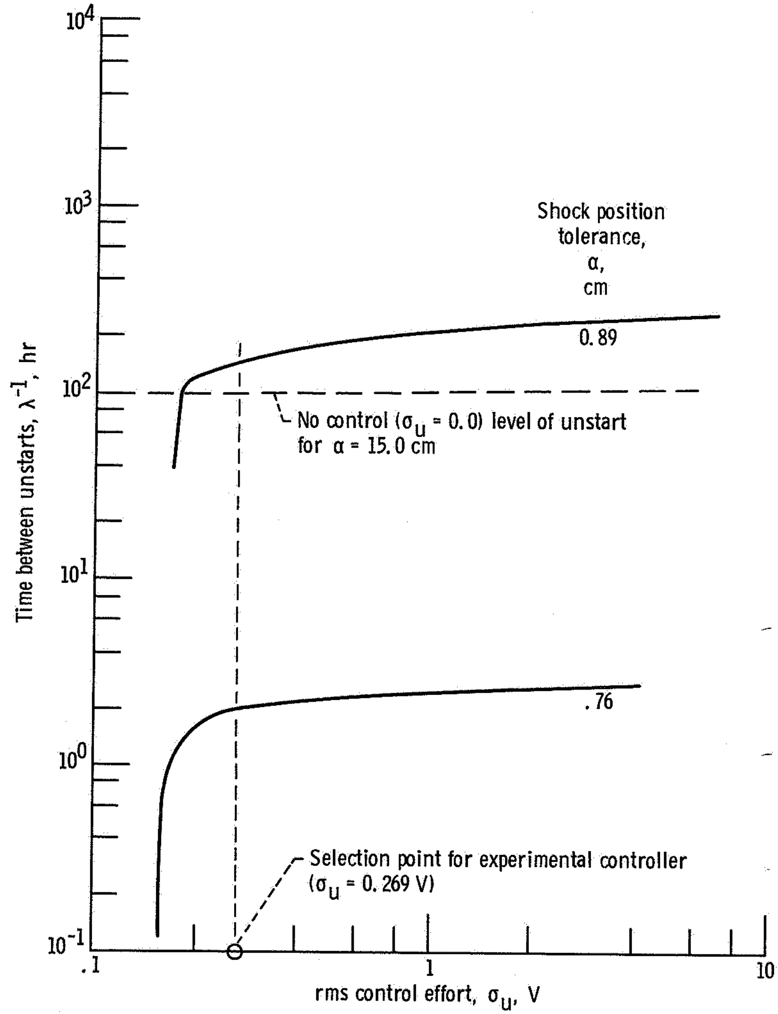

Figure 10. - Shock position feedback (SPF) case A unstart performance.

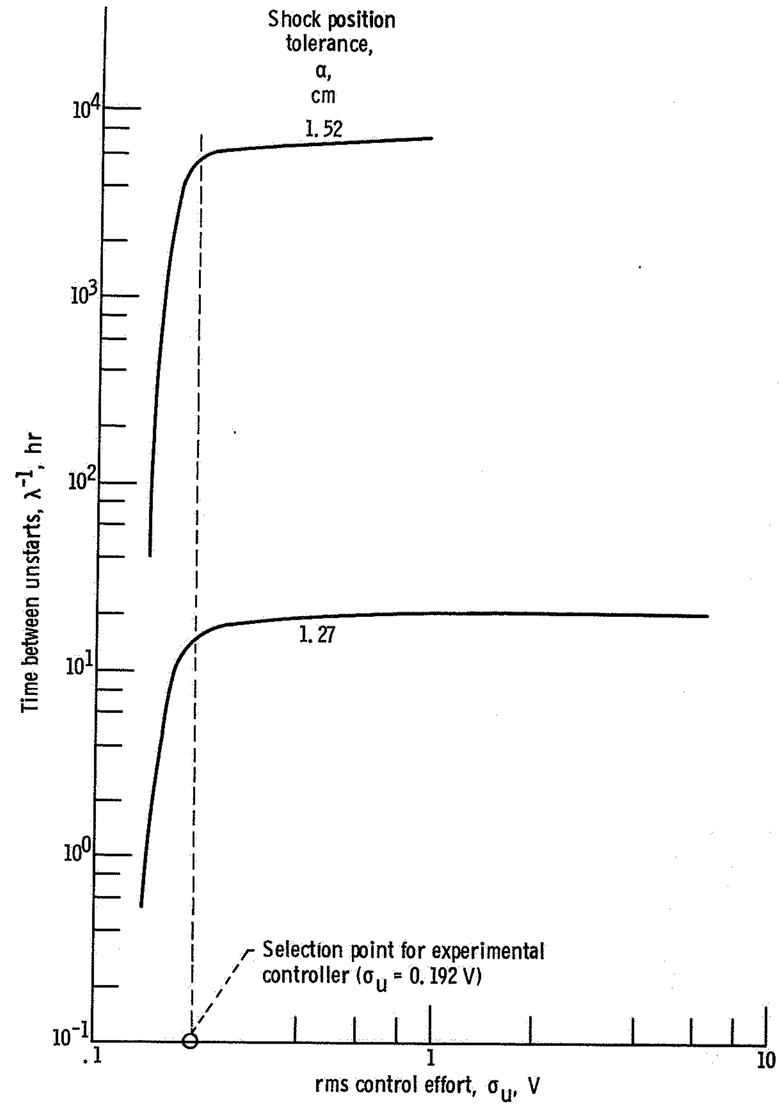

Figure 11. - Throat exit feedback (TEF) case A unstart performance.

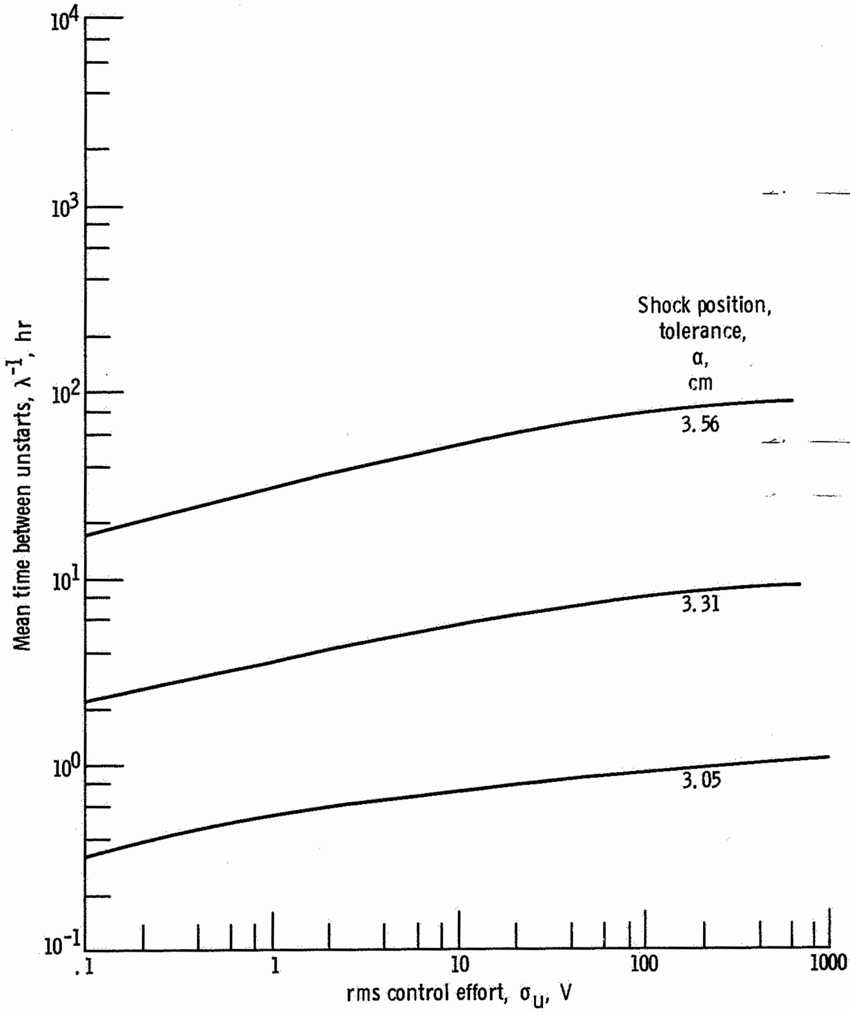

Figure 12. - Shock position feedback (SPF) case B unstart performance.

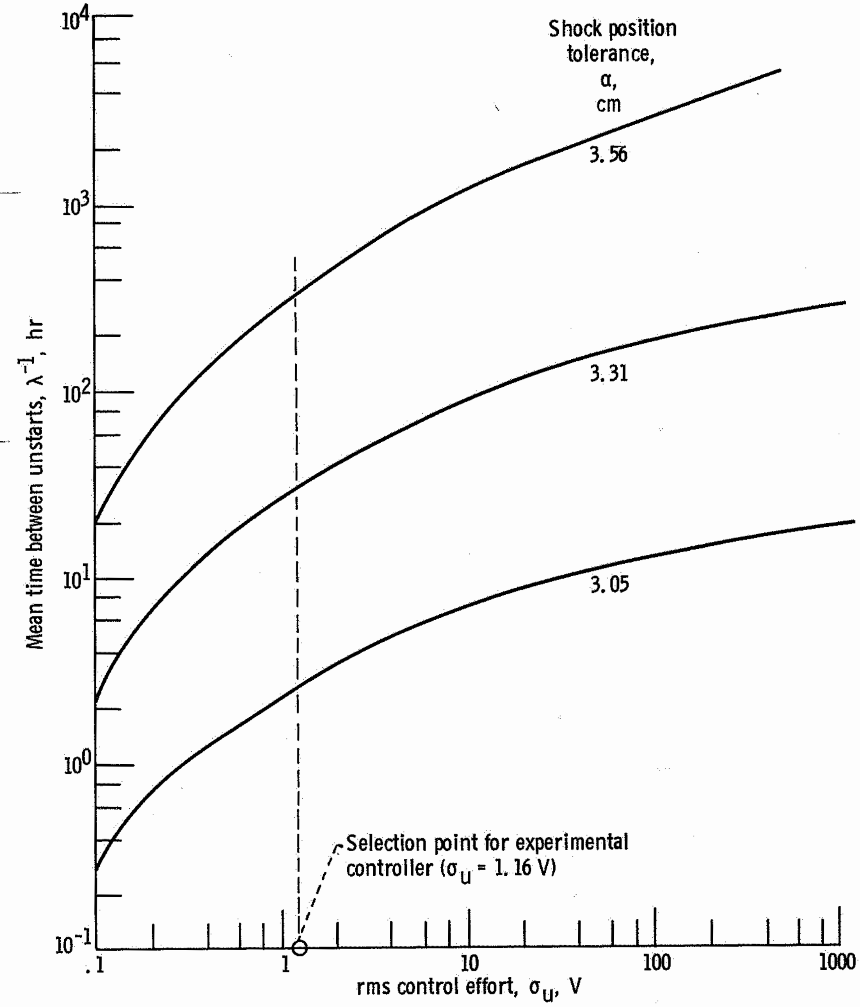

Figure 13. - Throat exit feedback (TEF) case B unstart performance.

15 centimeters, inlet overall performance (pressure recovery and distortion) would be considerably worse than with the setting of 0.89 centimeter possible with closed-loop control.

Figure 12 and 13 are unstart performances for the two feedback configurations (SPF and TEF) for the case B disturbance (high frequency content). The three α settings are the same for each configuration. When comparing these two figures it can be seen that there is a benefit from sensing the throat exit pressure p_{te} instead of shock position y_s. This signal is closer to the disturbance than shock position y_s, and, for the high-frequency (case B) disturbances, it shows unstart improvement. Even though the p_{te} signal is highly corrupted by measurement noise, the data of figure 13 show that the closeness of p_{te} to the higher frequency disturbance yields performance benefits. The need for less phase lag between disturbance and measurement seems to outweigh the measurement uncertainty where higher frequency disturbances are concerned.

Experimental Controller Selection

In the preceding sections the techniques for finding an optimal inlet controller for a nonquadratic performance index were presented. These techniques were applied to the design of optimal controllers for the 40/60 inlet, which were then evaluated in the SWT. Selection of the feedback gains (K_c) and estimator gains (K_e) for three of the four plant/noise configurations was made. The three configurations selected are

SPF system, case A disturbance (fig. 10)

TEF system, case A disturbance (fig. 11)

TEF system, case B disturbance (fig. 13)

For each of the three configurations one specific set of optimal controller gains corresponding to a specific value of rms control effort σ_u was selected. The values of σ_u at which the controller gains were selected are indicated in figures 10, 11, and 13. The actual selection was carried out in the following manner.

The physical variable used in selecting the control gains K_c was the control bypass airflow w_c. This variable has a well defined maximum value, determined by the maximum opening of the bypass doors. The airflow w_c is related to the bypass door actuator input u by the transfer function of equation (11). For each optimum controller, the rms value of control airflow σ_{w_c} was computed. The controller gains selected for experimental evaluation were those for which the resultant value of σ_{w_c} was equal to 0.168 kilogram per second. This value is equal to 10 percent of the rms bypass door flow capacity when operating about midposition.

It should be pointed out that the transfer function of equation (11) indicates the control airflow w_c is related to the input u as a function of frequency. Also, the inlet disturbance energy has some frequency distribution which causes some type of frequency distribution on the control signal u.

Therefore, even though the three experimental optimal controllers were selected for the same value of rms control airflow σ_{w_c}, the rms control efforts σ_u required to produce this fixed value of rms control airflow are different. This is indicated by the different values of σ_u appearing at the selection points in figures 10, 11, and 13. The vertical lines on these figures can be used to determine the unstart performance for the selected control designs.

The experimental results obtained using these selected controllers are presented and discussed in the EXPERIMENTAL CONTROLLER PERFORMANCE section.

EXPERIMENTAL CONTROLLER PERFORMANCE

Analog (Continuous) Controller

The state estimator - optimal controller configuration discussed in the CONTROLLER DESIGN AND ANALYTICAL PERFORMANCE section and shown schematically in figure 3 is described by the vector-matrix equations

$$\dot{\hat{x}} = A\hat{x} + K_e(z - H\hat{x}) + Bu \tag{16}$$

and

$$u = -K_c\hat{x} \tag{17}$$

These equations can be implemented directly by using analog computer components. Appendix B gives a brief description of the actual computer equipment employed in the experimental facility. As discussed earlier, three different optimal controller designs were experimentally evaluated. These designs involved two different measured variables described earlier as the SPF and TEF systems. Figures 4 and 5 show the general block diagrams for these two different configurations.

As can be seen from equations (16) and (17) and figure 3, the optimal controllers lend themselves quite naturally to hardware implementation with an electronic analog computer. The only difficulty involved in finalizing the analog hardware involved scaling the large values of estimator gains and control gains resulting from the design procedure. Most of the scaling problems were eliminated by using very fast integrating rates on each of the integrators. In the analog circuit, the outputs of various integrators were the system estimated states $\hat{x}(t)$. In this particular problem, the presence of transfer function zeros and the use of a Padé approximation for the dead time caused the state variables to differ from any actual system variables. Thus, the level or magnitude of state estimates during experimental system operation could not be easily predicted. This made analog scaling to prevent amplifier overloads very difficult. To resolve this problem, the experimental analog controllers were operated first with a linear analog simulation of the inlet system transfer functions. Scaling the estimated states was then adjusted to allow all the amplifiers to operate at satisfactory levels under the worse case levels of disturbance inputs. The results of operating the three designs with the experimental inlet in the wind tunnel (SWT) are presented in a later section.

Digital Computer (Discrete) Controller

Since a digital computer was already available in the SWT facility for a companion experimental controls program (ref. 16), it was decided to implement optimal control laws with a discrete controller. A brief description of the digital equipment is included in appendix B and a detailed description is in reference 17.

Presently the optimal inlet control is formulated and designed as a continuous controller. Equations (16) and (17) describing the optimal controller are linear, time-invariant, differential, and algebraic equations. Two possible approaches for designing optimal inlet controllers are available. One method involves transforming the inlet open-loop differential equations into discrete-time (difference) equations. Then a complete optimal control system can be designed in discrete time. Such an approach was not used, since for the inlet it would have required a new formulation of the optimal control solution as well as the development of new computer routines.

The other method for obtaining a digital computer control law involves approximating the continuous control law of equations (16) and (17) by difference equations. The performance of a system using a digital computer to implement these equations can be made equivalent to that possible with the continuous controller. This second method is the one selected for the program discussed in this report. The block diagram in figure 14 shows the manner in which the complete digital computer control system was implemented.

First, the appropriate measured output is sampled and converted to a digital equivalent upon which the computer can operate. During the uniform sampling interval T the computer algorithm is exercised and an optimal controller output u is obtained. This then is input to the control doors at the next sample time and it is held fixed for the duration of the sample period T. A sampling period of 1 millisecond was conservatively selected using the closed-loop stability criteria discussed in appendix D.

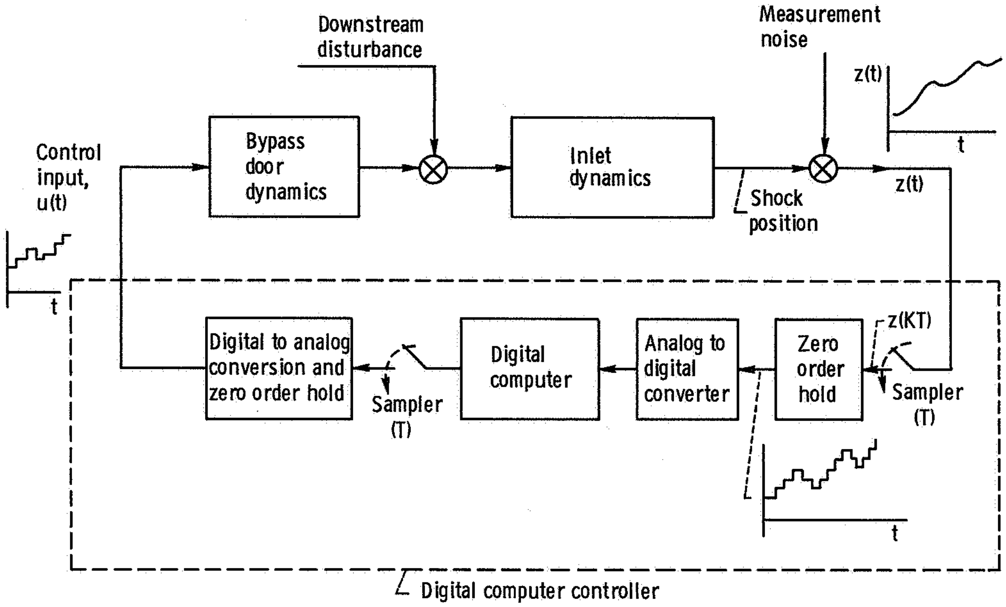

Figure 14. - Digital computer inlet control system block diagram.

Systems in which input and output controller information is sampled are called sampled-data control systems. Various techniques for analyzing such systems can be found in the literature. Both frequency domain approaches using the z-transform (refs. 18 and 19) and time domain approaches (refs. 15 and 20) have been used. Since the continuous formulation for the inlet problem is in the time domain, a time domain discrete formulation was obtained by using the state transition matrix (refs. 15 and 20).

For this particular control problem with ten estimated states which are not closely related to distinct physical variables, certain numerical programming problems were encountered. Techniques used to overcome these problems and arrive at an acceptable control algorithm are not included in this section since such details are not essential to a discussion of the experimental results. However, appendix D is included to discuss in detail the techniques involved in arriving at a practical computer control law.

The experimental performance of the discrete controller is presented in the next section along with the analog or continuous controller results.

Experimental Results and Discussion

In the experimental program, the system was subjected to sinusoidal airflow disturbances at the downstream end of the inlet as described in appendix B. Thus, all the performance data to be presented are in the form of closed-loop frequency responses of shock position to an airflow disturbance. The results show how well the controlled system regulates against sinusoidal disturbances of fixed amplitude at different distinct frequencies.

The test program would best have been run with random airflow disturbances as described by the spectral densities shown in figure 7. This was not done since the disturbance devices (bypass doors) would not have been capable of accurately duplicating these spectral densities. Also, to measure the frequency of unstarts to a random disturbance would have required considerable running time. This is impractical in the SWT.

Performing frequency response tests with fixed amplitude sinusoidal signal inputs is the technique used in past programs to evaluate controller experimental closed-loop performance. This is a direct way to look at linear time-invariant systems.

The experimental data presented in figures 15 to 23 consist of closed-loop frequency responses for the three controller designs discussed in the CONTROLLER DESIGN AND ANALYTICAL PERFORMANCE section. Also included are experimental open-loop frequency responses to evaluate the different controllers. For each controller, comparisons are made between the experimental and analytically predicted closed-loop frequency response performances. Analytical predictions of closed-loop performance are obtained as follows. Open-loop models of the inlet are defined by the finite-order transfer functions determined in appendix C and represented in the time domain by the matrices of tables II and III. A closed-loop system transfer function is derived and the frequency response is evaluated by using the open-loop models and the appropriate optimal gains K_c and state estimator. Also, where possible, comparison is made between the analog and digital computer implementations of the control laws.

Only frequency response magnitudes, not phase angles, are presented. All magnitude data are normalized to the open-loop magnitude at 1 hertz.

SPF system frequency response. - Figure 15 is a frequency response plot of the SPF case A controller design implemented with analog computer components. The uncontrolled or open-loop response of inlet shock position to a downstream airflow disturbance is also shown. It can be seen that control attenuates shock motion by a factor of at least 10:1 at frequencies of 0.5 hertz or less. However, as the disturbance frequency increases, the controller fails to attenuate the disturbance as well. In fact, from about 6 to 20 hertz it even amplifies the disturbance somewhat. Beyond this frequency, the shock position behaves as if the system were open loop. The case A disturbance, for which this particular control was designed, contains the majority of its disturbance energy at low frequencies. Thus, a large closed-loop attenuation is produced at the lower frequencies. The control design assumes what little disturbance energy exists at high frequency is sufficiently attenuated by the inlet duct dynamics; thus, the closed loop follows the open loop in this area. The slight amplification of shock motion from about 6 to 20 hertz probably does not significantly increase unstart frequency, since

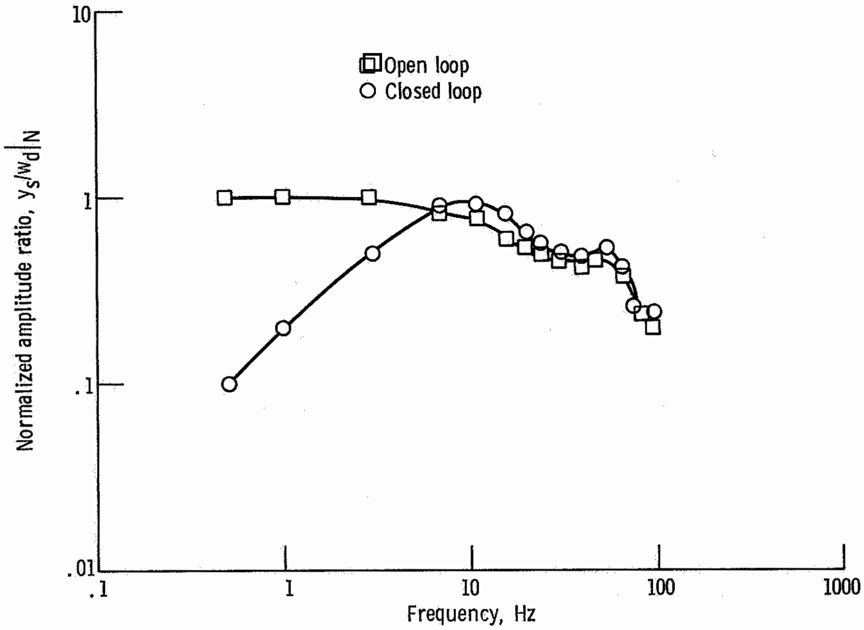

Figure 15. - Comparison of experimental open- and closed-loop frequency responses of shock position to disturbance airflow using SPF case A analog control.

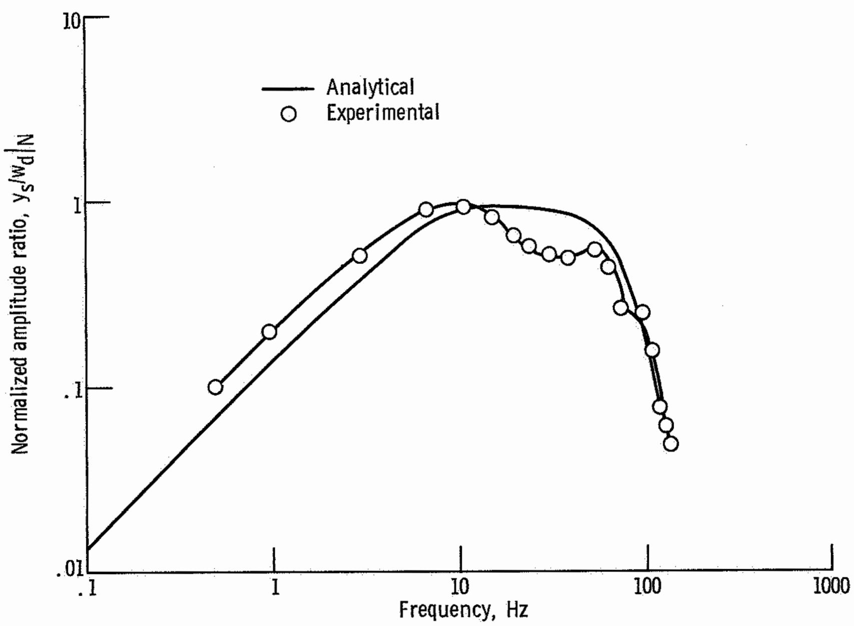

Figure 16. - Comparison of analytical and experimental closed-loop frequency responses of shock position to disturbance airflow using SPF case A analog controls.

disturbance energy in this band is small.

Figure 16 is a comparison of the analog SPF case A control experimental performance with the analytically predicted closed-loop performance. It can be seen that the analytical predictions show more attenuation at low frequency than the experimental values. It was found during the SWT tests that the shock position gain was about two-thirds the value used in modeling the plant (numerical values of table II) and designing the controller. This gain discrepancy is the most probable cause for the difference between the analytical and experimental performances especially at low frequency.

Figure 17 is a comparison between the experimental performance of the analog (continuous) and a digital computer (discrete) implementation of the SPF case A control design. The two implementations are, in general, quite similar except for some lack of low frequency disturbance attenuation with the digital version.

TEF system frequency response. - Figure 18 shows the experimental closed-loop frequency response of shock position to a disturbance when the TEF case A control design is implemented with analog components. The open-loop shock position response is included as a reference. Compared with the shock position feedback system shown in figure 15, low frequency attenuation is not quite so good. However, as frequency increases, the TEF system does better in the 6 to 20 hertz range. Since there is less lag between the p_{te} signal and the disturbance than between y_s and the disturbance, it is expected that this system might have an easier job of attenuating disturbances at the higher frequencies where phase lag is becoming a problem. Beyond 20 hertz, however, the system appears open loop. Again, this is because for case A little disturbance energy exists in this region.

Figure 19 compares the experimental and analytical frequency responses of the analog version of TEF case A control. Responses compare very well out to 20 hertz. After 20 hertz the comparison is not good. The probable cause is that beyond this frequency the analytical inlet model used for design and prediction was not an extremely close fit on amplitude. This can be seen by looking at figures of the curve fit information of figure 3 in appendix C. A more accurate fit would probably have produced closer agreement between experimental and analytical results.

Figure 20 is a comparison of the closed-loop shock position frequency response of the analog and digital computer versions of the TEF case A control design. The two responses are almost identical. As stated earlier, the digital control algorithm was designed for and used a sampling time of 1 millisecond. This is quite adequate for disturbance frequencies up to 100 hertz; therefore, the close correlation with the continuous analog version as shown in figure 20 is as expected.

Figure 21 presents the closed-loop frequency response of the analog TEF case B controller design. Also shown is the inlet open-loop frequency response. It should be remembered that case B has a certain amount of disturbance energy in the midfrequency range and not as much at the very low frequencies. As a result, the controller perform-

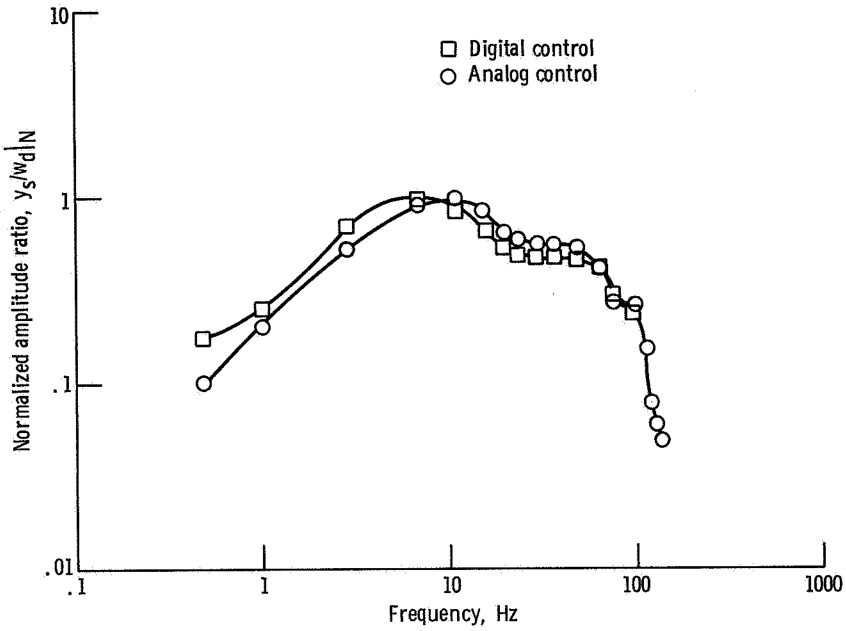

Figure 17. - Comparison of closed-loop experimental frequency responses of shock position to disturbance airflow using SPF case A analog and digital controls.

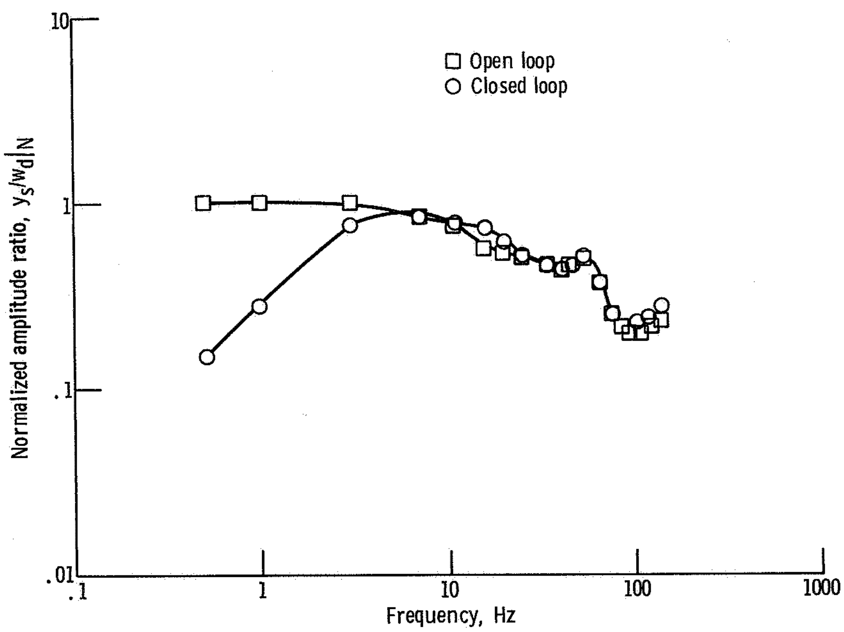

Figure 18. - Comparison of experimental open- and closed-loop frequency responses of shock position to disturbance airflow using TEF case A analog control.

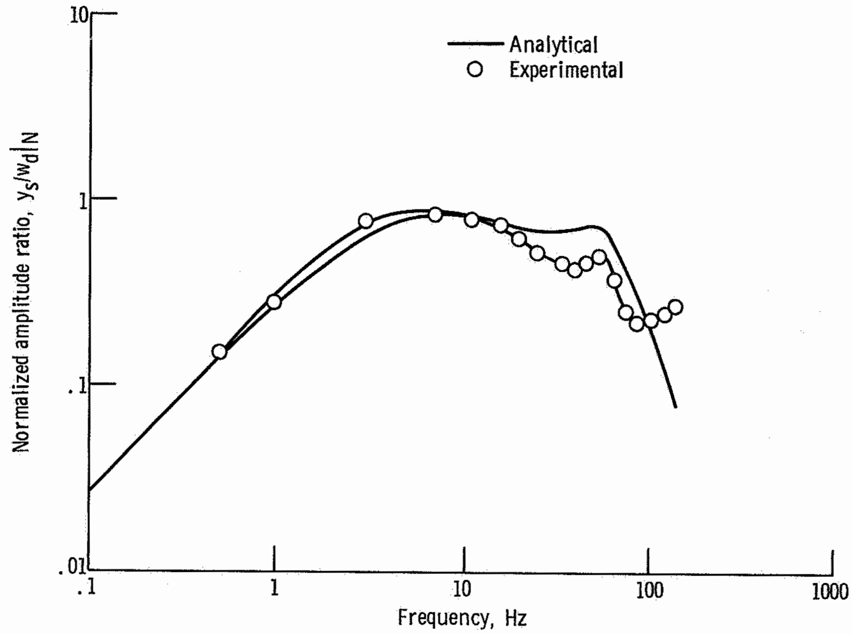

Figure 19. - Comparison of analytical and experimental closed-loop frequency responses of shock position to disturbance airflow using TEF case A analog controls.

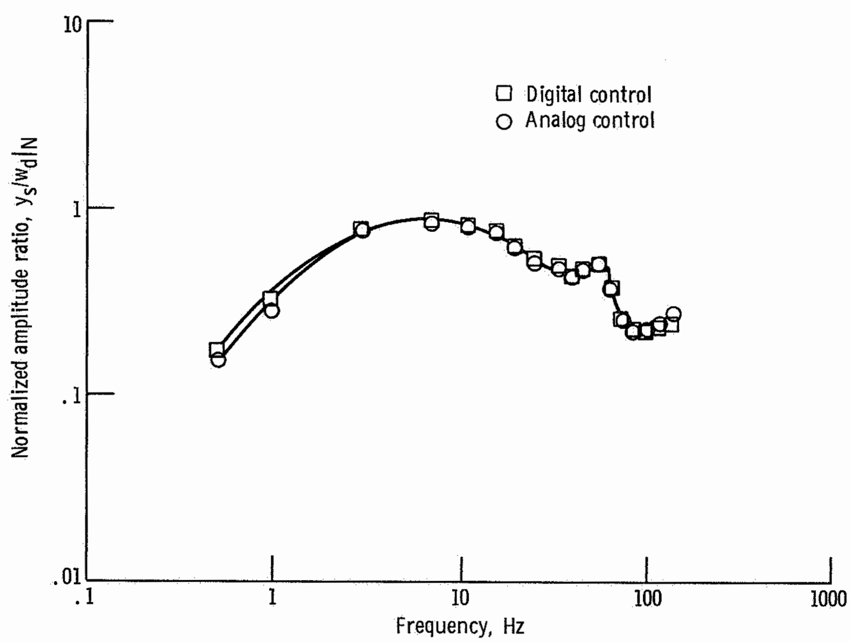

Figure 20. - Comparison of closed-loop experimental frequency responses of shock position to disturbance airflow using TEF case A analog and digital controls.

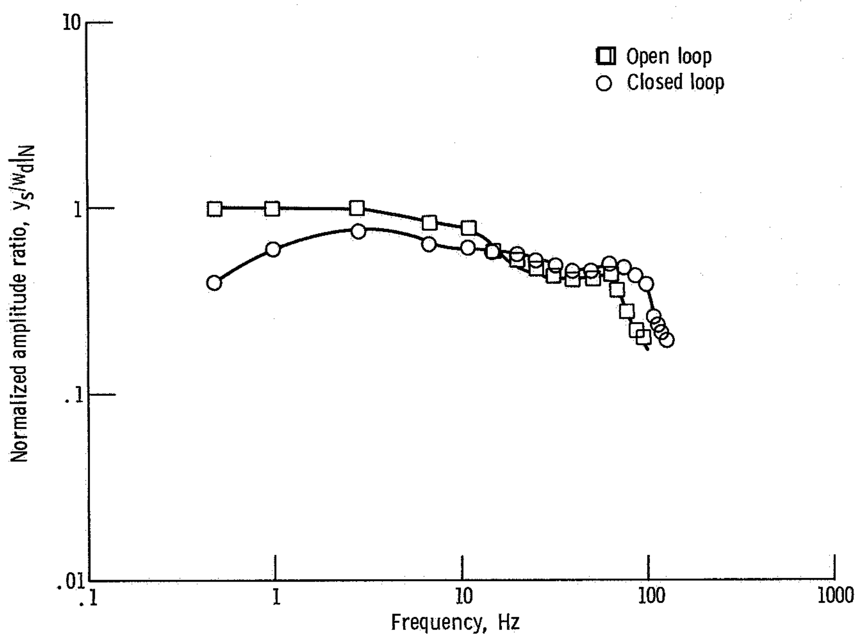

Figure 21. - Comparison of open- and closed-loop experimental frequency responses of shock position to disturbance airflow using TEF case B analog control.

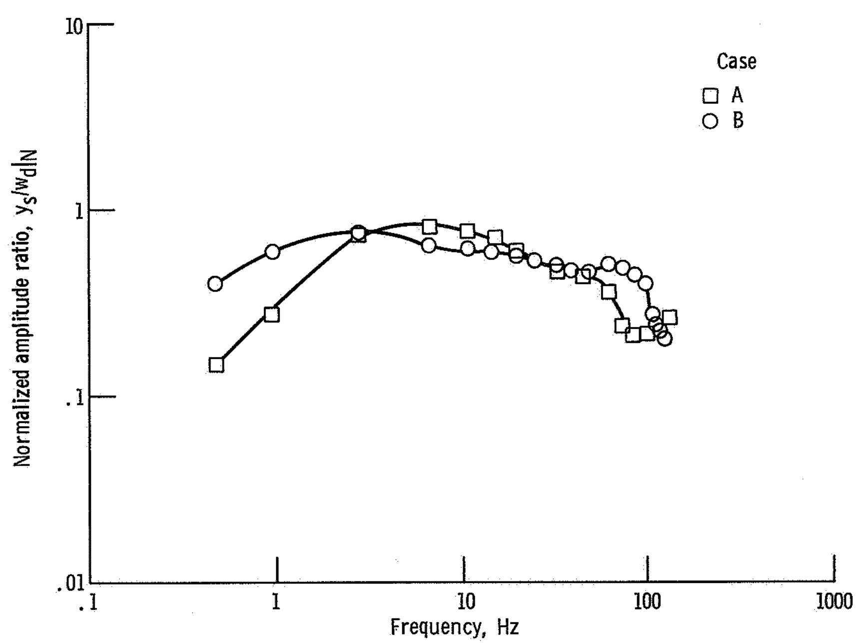

Figure 22. - Comparison of case A and case B closed-loop experimental frequency responses of shock position to disturbance airflow using TEF analog controls.

ance shown in figure 21 does not attenuate the low frequency disturbances as much as either of the case A controllers, but it does produce more attenuation in the midfrequencies out to about 20 hertz. This is shown by figure 22 which compares experimental analog versions of the TEF system for both the case B and case A designs. Case A provides very little attenuation after 3 to 4 hertz, whereas the case B design "keeps working" out to 20 hertz. The slight magnification over the open loop shown in figure 21 is difficult to explain except that control in this region is quite difficult because of the great deal of phase lag from the inlet at these frequencies.

Figure 23 presents a comparison of the experimental response of the analog TEF case B design and its analytical counterpart. The prediction is quite good, especially

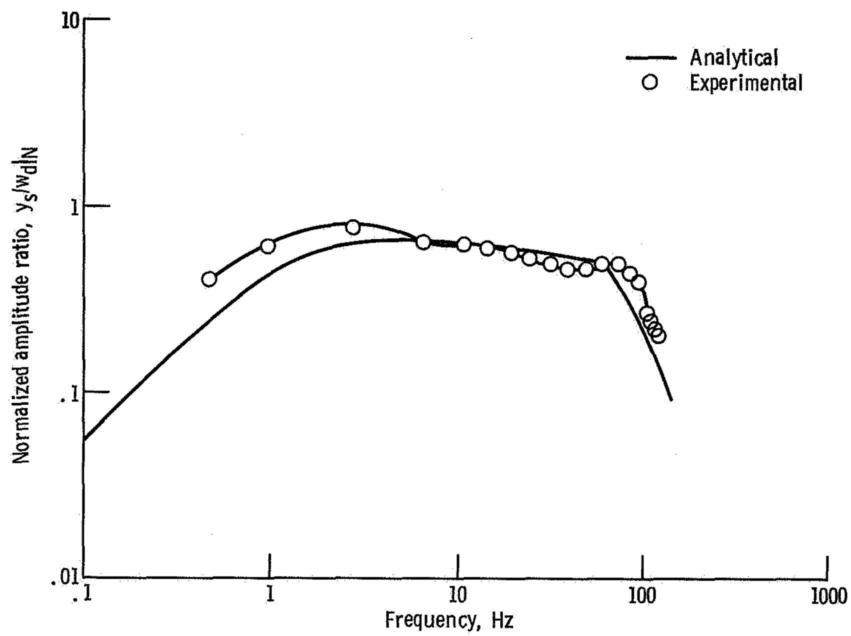

Figure 23. - Comparison of closed-loop analytical and experimental frequency responses of shock position to disturbance airflow using TEF case B analog controls.

in the midfrequency range. In the area of 80 to 100 hertz the analytical prediction shows better disturbance attenuation than the experimental. This is probably due to the limited order inlet model used in the analytical design. The additional phase shift of the actual inlet causes the experimental data to be somewhat degraded in this region.

Summary of experimental results. - To summarize the experimental data, several observations can be made. In general, the three controller designs performed in agreement with their analytical predictions except for the shock feedback system SPF, where a difference in inlet model gain was found to exist. Each of the three controllers was implemented with an analog computer. Only two of the three were put into discrete form and implemented with a digital computer. Where the two were compared to their analog counterparts, equivalency was quite good. In general, the experimental program pointed out the problems of designing and then implementing linear optimal controller designs.

Conclusions and Recommendations

It has been demonstrated that inlet controllers which minimize the expected frequency of unstarts can be designed and implemented. It was shown that controller characteristics depend strongly on the spectrum of the disturbance. Both shock position (SPF) and throat exit static pressure (TEF) were used as feedback variables. Because of the difference in noise levels on these signals, it was found that SPF was better for disturbances rich in low frequencies and TEF was better for higher frequency disturbances.

Analytically predicted and experimental closed-loop frequency responses were found in general to be in close agreement. Experimental controllers were implemented with both an analog computer and a digital computer. Analog and digital results compared quite favorably.

This attempt at applying linear stochastic optimal control theory to inlet control problems has, therefore, met with some success. The possible benefits which can be gained from using this relatively new theory seem to be great. However, this investigation exploited only a small fraction of the capabilities of the stochastic optimal control design approach. The remainder of this section contains recommendations as to areas that might warrant further investigation, both analytically and experimentally:

(1) Consideration should be given to designing an optimal controller for both shock position and throat Mach number for both atmospheric and compressor face disturbances. This problem could use the multiloop capabilities of the optimal control design technique.

(a) Multiple measurements could be used: throat exit and compressor face pressure, throat Mach number, cowl lip Mach number, etc. Experiments would be needed to determine more precisely various measurement channel noise levels and spectrum of the compressor face disturbance.

(b) Controlled variables such as spike position (and possibly engine speed) as well as bypass door opening should be considered.

(c) A quadratic performance index could be used involving mean-square values of shock position and throat Mach number plus penalties on bypass door opening, spike position, actuator slewing velocities, etc.

(2) Sensitivity studies should be conducted on future inlet controller designs to determine the degradation in performance when inlet or noise parameters vary from those assumed in the design process.

(3) Controllers developed in the present study tended to be somewhat complex. Therefore, methods of developing simpler optimal or suboptimal controllers should be studied. Some approaches might be as follows:

(a) Reduce the order of the open-loop inlet model and compare the results (on the more complete inlet model) using controllers based on the lower order model with those of the more complex model.

(b) Investigate techniques of simplifying controllers which have been designed for the complete inlet model.

(4) The approach used in this study for digital control is not unique; thus, alternate approaches to optimal digital computer control of inlets should be studied. The goal is to increase the sampling period while achieving performance comparable to continuous-type control. This could be done by:

(a) Studying various ways of discretizing inlet and/or controller differential equations.

(b) Developing a method for directly determining the optimal discrete-time control law for a continuous-time system.

Lewis Research Center,
National Aeronautics and Space Administration,
Cleveland, Ohio, November 10, 1972,
501-24.

APPENDIX A

SYMBOLS

A	system matrix, $n \times n$
B	control matrix, $n \times c$
C	output matrix, $l \times n$
c	dimension of u
D	plant disturbance matrix, $n \times d$
d	dimension of w
$G_{BPD}(s)$	bypass door transfer function, (kg/sec)/V
$G_{DUCT}(s)$	inlet duct transfer function, $(N/cm^2)/(kg/sec)$
$G_{INLET}(s)$	overall inlet transfer function, cm/(kg/sec)
$G_{NS}(s)$	noise shaping transfer function, ND
$G_{SHOCK}(s)$	inlet shock position transfer function, $cm/(N/cm^2)$
H	measurement matrix, $m \times n$
I	identity matrix
J	performance index
J_{eq}	equivalent quadratic index
K_c	control gain matrix, $c \times n$
K_e	estimator gain matrix, $n \times m$
k	weighting factor
l	dimension of y
m	dimension of z
n	dimension of x
P	diagonalization transformation matrix
p	pressure, N/cm^2
p_{te}	throat exit static pressure, N/cm^2
q	transformed state vector, $n \times m$
r	number of terms in truncated series

s	Laplace variable, sec^{-1}
T	sampling period, sec
t	time, sec
u	control vector, $c \times 1$
v	measurement noise vector, $m \times 1$
v_{y_s}	shock position measurement noise, cm
$v_{p_{te}}$	throat exit static measurement noise, N/cm^2
W_1	equivalence coefficient
W_2	equivalence coefficient
w	plant disturbance vector, $d \times 1$
w_c	control airflow, kg/sec
w_d	compressor face disturbance airflow, kg/sec
w_i	total inlet airflow, kg/sec
x	state vector, $n \times 1$
y	output vector, $l \times 1$
y_s	shock position, cm
Z	arbitrary square matrix
z	measurement vector, $m \times 1$
α	shock position tolerance, cm
$\left.\begin{matrix}\alpha_1\\ \alpha_2\\ \alpha_3\end{matrix}\right\}$	noise shaping transfer function parameters, rad/sec
Γ_{ce}	discrete estimator control input vector, $n \times c$
Γ_m	discrete measurement vector input to estimator, $n \times m$
Γ_{cp}	discrete plant control input vector, $n \times c$
Γ_d	discrete disturbance vector, $n \times d$
λ	expected frequency of unstarts, unstarts/sec
φ_{CL}	closed loop discrete state transition matrix, $2n \times 2n$
φ_e	estimator discrete state transition matrix, $n \times n$
φ_p	plant discrete state transition matrix, $n \times n$

σ_u RMS control effort, V

σ_u^2 mean-square control effort, V^2

$\sigma_{w_c}^2$ mean-square value of control airflow, $(kg/sec)^2$

$\sigma_{w_d}^2$ mean-square value of disturbance airflow, $(kg/sec)^2$

$\sigma_{y_s}^2$ mean-square shock position, cm^2

$\sigma_{\dot{y}_s}^2$ mean-square shock velocity, $(cm/sec)^2$

τ dummy variable

τ_d transportation lag, sec

Superscripts:

$\cdot$ differentiation with respect to time

$*$ trial values

$\hat{}$ optimal estimate of a vector

T transpose

Operators:

PSD( ) power spectral density of

$(\,)\big|_N$ normalized to 1 Hz

APPENDIX B

APPARATUS AND PROCEDURE

Inlet Description

The inlet used for the investigation was an axisymmetric mixed compression type with 60 percent of the supersonic area contraction occurring internally at the design Mach number of 2.5. A cutaway view of the NASA designed inlet is shown in figure 24. Specific characteristics of the inlet as well as the tunnel test conditions are tabulated in table IV. Additional aerodynamic design details and steady-state performance characteristics of the inlet are given in references 21 and 22. The dynamic responses of various inlet internal pressures and of normal shock position to airflow disturbances are reported in reference 6.

Shown in figure 24 are the inlet's translating centerbody and overboard bypass doors of which there are a total of six. Both the bypass doors and centerbody are hydraulically actuated and electronically controlled. Three of the symmetrically located bypass doors,

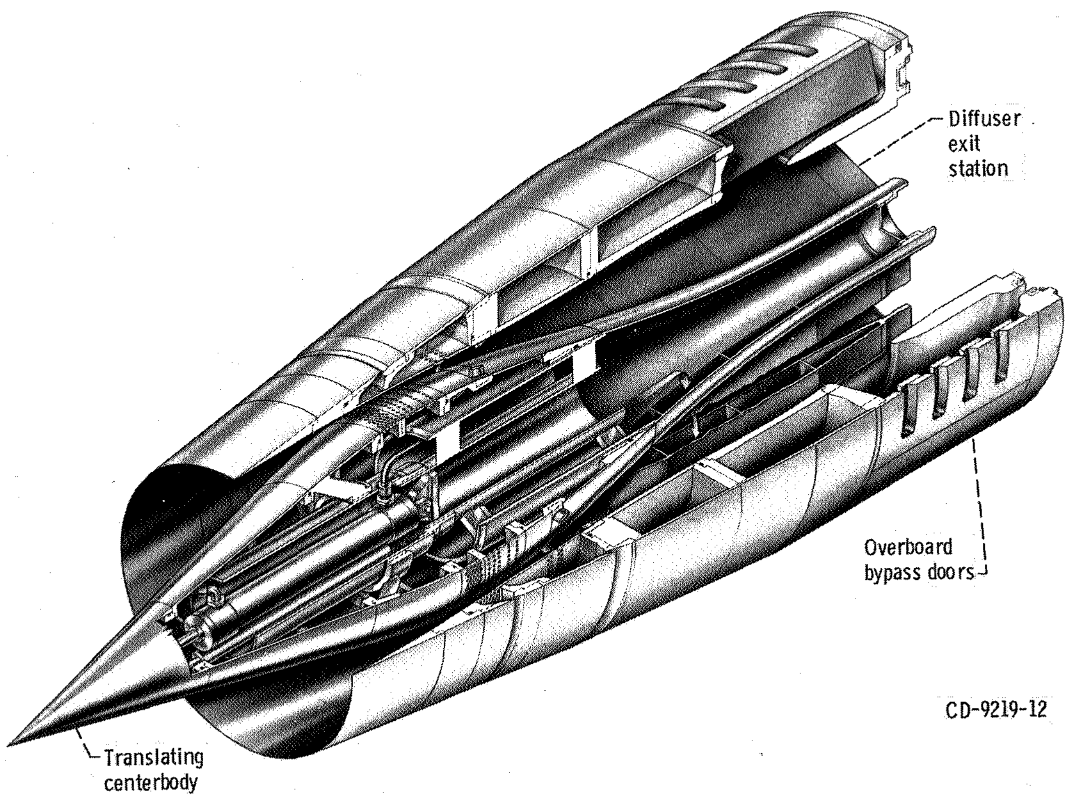

Figure 24. - Cutaway view of inlet model.

TABLE IV. - DETAILED INLET SPECIFICATIONS

AND TUNNEL TEST CONDITIONS

Inlet	
Cowl lip diameter, cm	47.3
Capture area, cm^2	1760
Capture corrected airflow, kg/sec	16.2
Tunnel test conditions	
Mach number	2.5
Total temperature, K	315
Total pressure, N/cm^2	8.95
Specific heat ratio	1.4
Reynolds number (based on cowl-lip diameter)	3.88×10^6
Angle of attack, deg	0
Inlet orifice termination description	
Choke plate area, cm^2	598
Flow coefficient	0.985
Location of choke plate from cowl lip, cm	146.5

driven in parallel, were used to provide sinusoidal disturbances in diffuser exit corrected airflow. The remaining three bypass doors, also driven in parallel, were used as the manipulated variable of the various normal shock controllers.

Inlet Instrumentation

Figure 25 indicates the location of pressure taps connected to dynamic strain gage pressure transducers used in the investigation. The pressure transducers were close coupled to the pressure taps to enhance their response capabilities. Details of the location, response, and usage of the pressure sensors are documented in references 8 and 16.

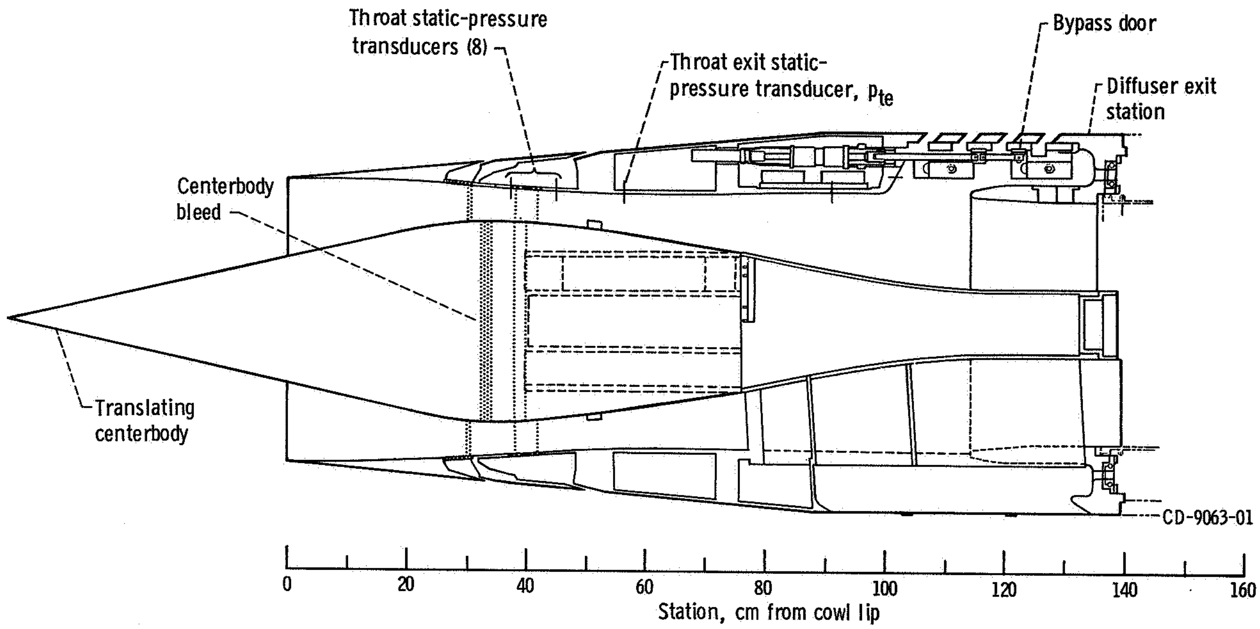

Figure 25. - Details of inlet including instrumentation locations.

Shock Sensing

In this program eight throat static pressure signals were used as inputs to an electronic normal shock position sensor. The logic required for this sensor was implemented on both a general purpose analog computer and on a digital computer. The design details of this sensor are discussed in references 12 and 16. The output produced by either implementation was a stepwise continuous signal indicative of shock position. The various shock position controls tested used either the throat exit static pressure p_{te} or the stepwise continuous shock position sensor as the feedback signal for control.

Controller Implementation

The inlet controllers designed by modern control techniques were implemented on both a general purpose analog computer and on a digital computer.

Figure 26 is a photograph of the general purpose digital computer used for implementation of both inlet and engine controls. The system, shown in block diagram form in figure 27, consists of four major units:

1. A digital computer with 16 384 words of memory, a read-restore memory cycle time of 750 nanoseconds, and a word length of 16 bits
2. A digital interface capable of converting both analog and frequency signals to computer compatible digital words and converting computer generated words to analog and logical outputs

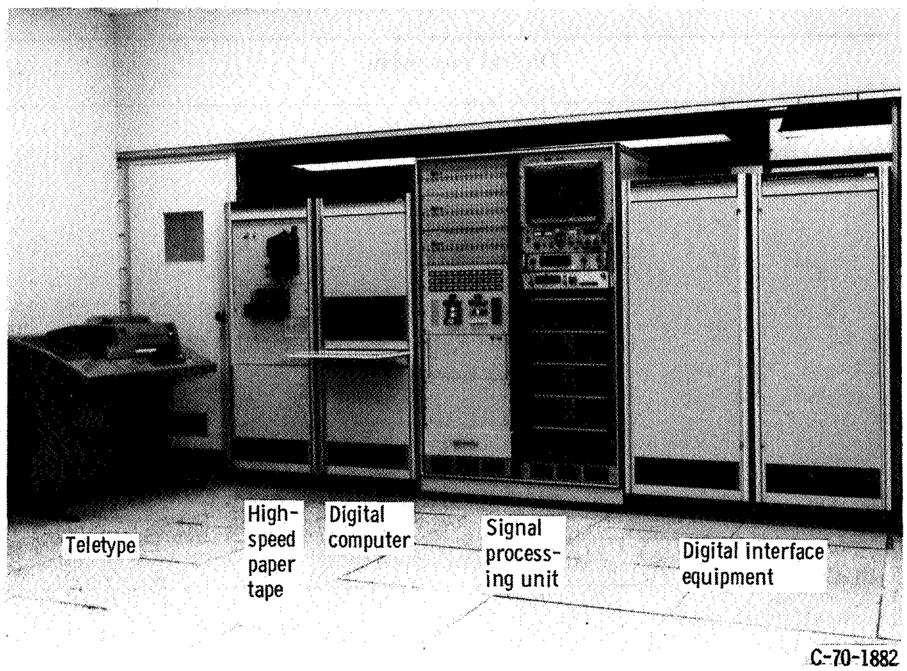

Figure 26. - Digital control computer system.

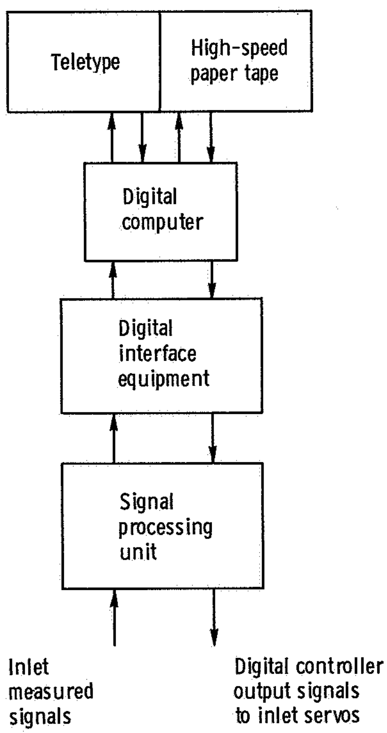

Figure 27. - Schematic of digital computer setup.

TABLE V. - DIGITAL CONTROL COMPUTER SYSTEM CAPABILITIES

Digital computer	
Magnetic core memory size, words	16 384
Word length, bits plus parity	16
Memory cycle time, nsec	750
Add time, μsec	1.5
Multiply time, μsec	4.5
Divide time, μsec	8.25
Load time, μsec	1.5
Indirect addressing	Infinite
Indexing	Total memory
Priority interrupts	28 separate levels
Index registers	2
Interval timers	2
Analog acquisition unit	
Overall sample rate (maximum), kHz	20
Resolution of digital data, bits	12 (plus sign)
Output code	Two's complement
Number of channels	64
Input range, V full scale	±10
Conversion time, μsec	38
Total error with calibration, percent	0.073
Analog output unit	
Total number of digital-to-analog conversion channels (DAC)	26
Resolution 13 bit DAC (10 channels), bits (12+1)	12 (plus sign)
Accuracy (13 bit) DAC, percent of full scale	±0.05
Resolution 12 bit DAC (16 channels), bits (11+1)	11 (plus sign)
Accuracy (12 bit DAC), percent of full scale	±0.1
Output voltage range, V full scale	±10
Slew rate, V/μsec	1
Priority interrupt processor	
Number of channels	10
Input voltage range, V	±10
Computer switching	Trigger on rise or fall
Comparator hysteresis, mV	Adjustable from 35 to 650
Comparator output, V	7

3. A signal processing unit which provides signal conditioning and monitoring capability between the digital interface and the propulsion system to be controlled
4. Programming peripherals consisting of a high-speed, paper-tape reader and punch and a teletype

The capabilities of the system are given in table V and a comprehensive description is available in reference 17.

All inlet pressure measurements were passed through signal conditioners and isolation amplifiers to provide high-level (-10 to +10 V) inputs to the digital interface equipment. This unit contains a random access multiplexer, a sample and hold amplifier, and a 13-bit digitizer. The complete digitizing process from channel sample command to entry of the digitized measurement into computer memory requires 50 microseconds. This process is automated through the use of a block data transfer unit which ties up the main frame for only one memory cycle per word transferred. Completion of the sampling process is conveyed to the computer by a priority interrupt from the block data transfer unit.

Digital commands are issued directly from the computer main frame to the 13-bit digital-to-analog converters. These outputs are passed through isolation amplifiers to provide ground isolation of the digital system and then to the servoamplifiers driving the manipulated variables.

Test Procedures

Both open-loop (no input to control bypass doors) and closed-loop frequency response tests were run. For all tests, the steady-state operating point of the normal shock was located near the middle of the eight throat static pressure taps. This was accomplished with an appropriate steady-state setting of the six bypass doors. An appropriate disturbance amplitude was determined from the open-loop response tests. For the open-loop tests, the three disturbance doors were oscillated sinusoidally at an amplitude sufficient to move the normal shock over the eight throat static taps (fig. 25) at 1 hertz. This was the disturbance amplitude used at all frequencies for both the open- and closed-loop testing. In addition to open-loop tests, closed-loop frequency response tests were run using both the throat exit static pressure p_{te} and the stepwise continuous shock position sensor output as measured variables. These tests were intended to determine the capability of the feedback controllers to regulate inlet shock position in the presence of compressor face disturbances.

For the frequency response tests, both magnitude and phase data for a few significant signals were determined online using a commercial frequency response analyzer in the control room. These signals, as well as many others, were recorded in analog form on magnetic tape for reduction at a later time. All frequency response data were plotted in the form of Bode plots. The magnitude response data were normalized to the magnitude at 1 hertz.

APPENDIX C

FREQUENCY RESPONSE CHARACTERISTICS OF THE UNCONTROLLED (OPEN-LOOP) 40/60 SUPERSONIC INLET

A general physical description of the mixed compression (40/60) inlet used for the program discussed in this report is presented in appendix B (figs. 24 and 25). Frequency response data describing the dynamic characteristics of this inlet were obtained in the test programs described in references 7 and 8. Figure 28 describes in block diagram form the particular inlet transfer functions which were obtained. Figure 28 indicates that an incremental airflow disturbance w_i occurring at the downstream or compressor face end of the inlet will propagate upstream, resulting in a pressure variation at the throat exit (p_{te}) pressure sensor location. It will also cause motion of the normal shock y_s about its quiescent or desired steady-state location.

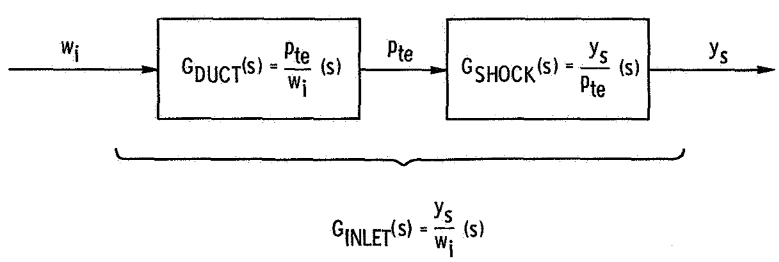

Figure 28. - Block diagram of inlet characteristics to downstream airflow disturbance.

The data presented in this appendix are used as a basis for determining transfer function relations G_{DUCT}, G_{INLET}, and G_{SHOCK} which approximately describe the inlet. These relations serve as a starting point with which to undertake the control design in the CONTROLLER DESIGN AND ANALYTICAL PERFORMANCE section.

Shock Position Measurement Model ($G_{INLET}(s)$)

The first configuration to be considered is the overall inlet response of shock position y_s to the disturbance w_i. The data points in figure 29 show the experimental amplitude and phase frequency response performance of the inlet shock position y_s to the airflow disturbance w_i at the compressor face station. The amplitude data have been normalized to the value at 1 hertz. To ensure the linearity required for future transfer

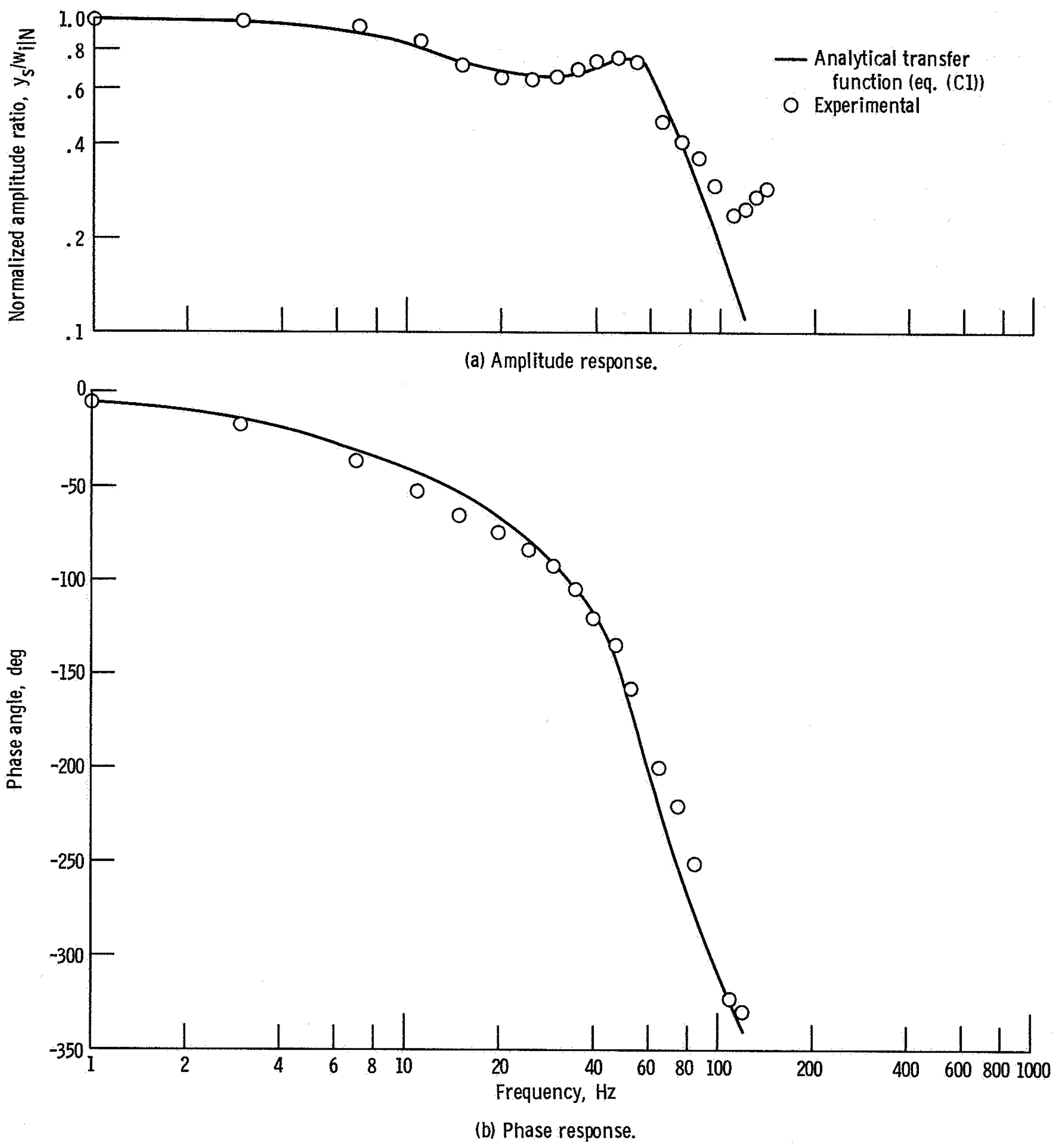

Figure 29. - Comparison of analytical and experimental frequency response performance of shock position to inlet airflow.

function representations of the inlet frequency response data, the airflow disturbance w_i was of a small enough amplitude to encounter as few nonlinear effects as possible.

An analytical representation of the experimental data presented in figure 29 was obtained by curve fitting the frequency response characteristics of an approximate transfer function model to the amplitude and phase data. Equation (C1) is the result of the curve-fitting effort:

$$G_{INLET}(s) = \frac{y_s}{w_i}(s) = \frac{16.25\left(\frac{s}{210} + 1\right)e^{-4.0\times10^{-3}s}}{\left(\frac{s}{80} + 1\right)\left(\frac{s^2}{365^2} + \frac{0.6s}{365} + 1\right)} \quad \frac{cm}{kg/sec} \qquad (C1)$$

Included in this equation is the steady-state gain relation for the inlet. The solid lines of figure 29 give the frequency response of equation (C1), where the amplitude response has been normalized to the amplitude response at 1 hertz. The approximation of equation (C1) is quite good out to 100 hertz for both amplitude and phase. Beyond 100 hertz the amplitude response of the approximation falls off and deviates from the experimental data while the phase angle is still reasonably accurate. The approximation could, of course, be improved by the addition of more poles and/or zeros to the transfer function $G_{INLET}(s)$ of equation (C1). It is felt, however, that improved higher frequency (100 to 200 Hz) model accuracy at the expense of increasing the complexity of equation (C1) was not warranted.

Throat Exit Static Pressure Measurement Model ($G_{DUCT}(s)$ and $G_{SHOCK}(s)$)

The second configuration to be considered is a model which involves two distinct frequency response relations. These are the relations of the shock position measurement to a variation in the throat exit static pressure and the variation of p_{te} to a compressor face disturbance w_i.

The data points of figure 30 show the experimental frequency response of the throat exit static pressure p_{te} to the disturbance w_i. The coefficients in the transfer function of equation (C2) were found by curve fitting the data of figure 30:

$$G_{DUCT}(s) = \frac{p_{te}}{w_i}(s) = \frac{1.52\left(\frac{s}{210} + 1\right)\left(\frac{s}{500} + 1\right)e^{-1.5\times10^{-3}s}}{\left(\frac{s}{80} + 1\right)\left[\left(\frac{s}{365}\right)^2 + \frac{2(0.3)s}{365} + 1\right]} \quad \frac{N/cm^2}{kg/sec} \qquad (C2)$$

The frequency response performance of equation (C2) is given by the solid lines of figure 30. The amplitude response fits well to about 80 hertz at which point it drops off and does not duplicate the resonances of the experimental inlet data. The phase angle response in figure 30(b) is quite good to 140 hertz. The approximation therefore is felt sufficiently accurate for the purpose of controls design.

The data points in figure 31 show the experimental frequency response of shock position y_s to the pressure p_{te}. Since all frequency response information was determined by an airflow disturbance w_i at the compressor face, the data in figure 31 were obtained by finding the difference between the experimental data in figures 29 and 30. The transfer function approximation which was curve fit to the data in figure 31 is given by

$$G_{SHOCK}(s) = \frac{y_s}{p_{te}}(s) = \frac{10.68e^{-2.5\times10^{-3}s}}{\left(\frac{s}{500} + 1\right)} \quad \frac{cm}{N/cm^2} \qquad (C3)$$

The frequency response performance of equation (C3) is given by the solid curves in figure 31.

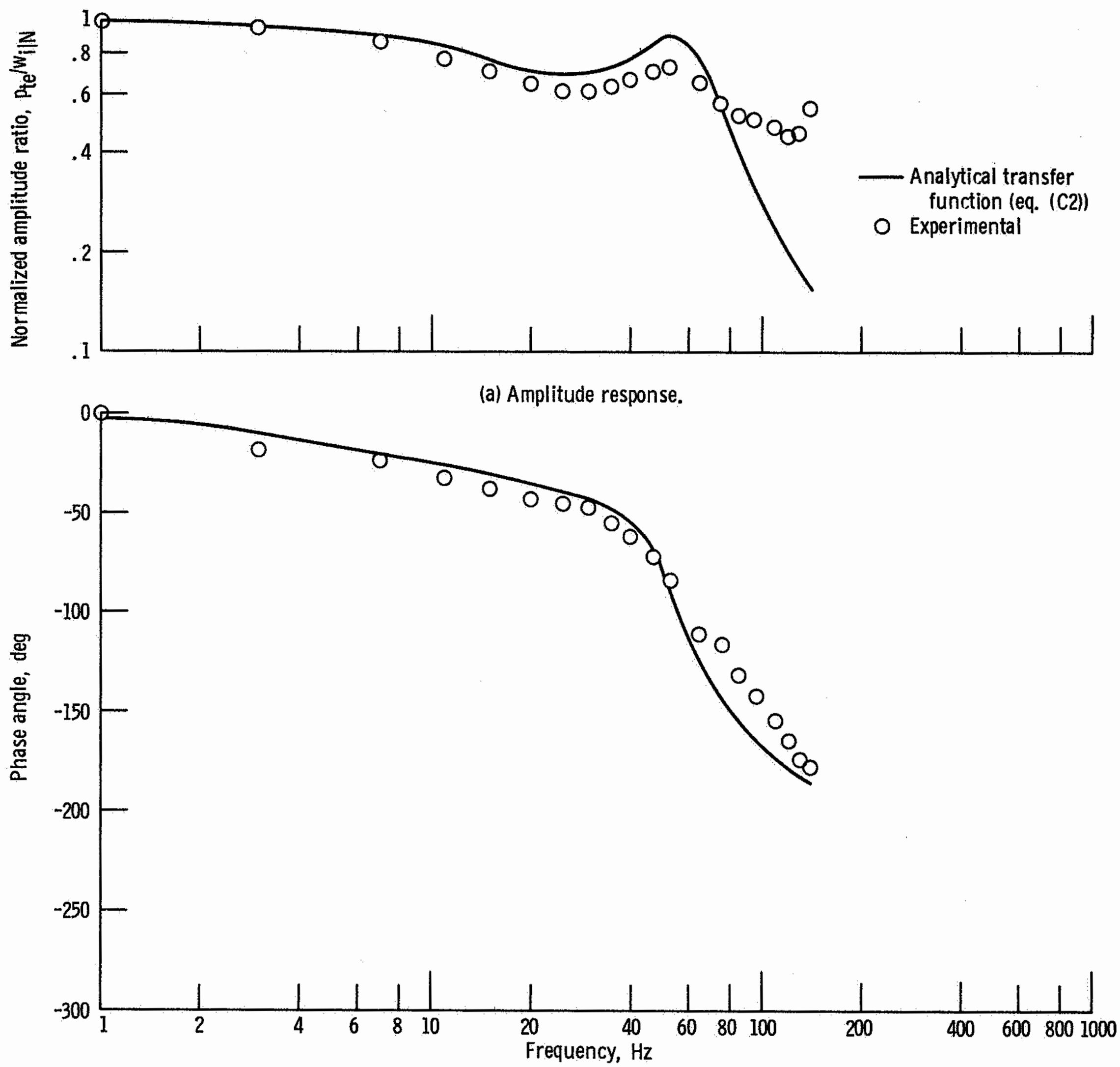

(a) Amplitude response.

(b) Phase response.

Figure 30. - Comparison of analytical and experimental frequency response performance of p_{te} to inlet airflow.

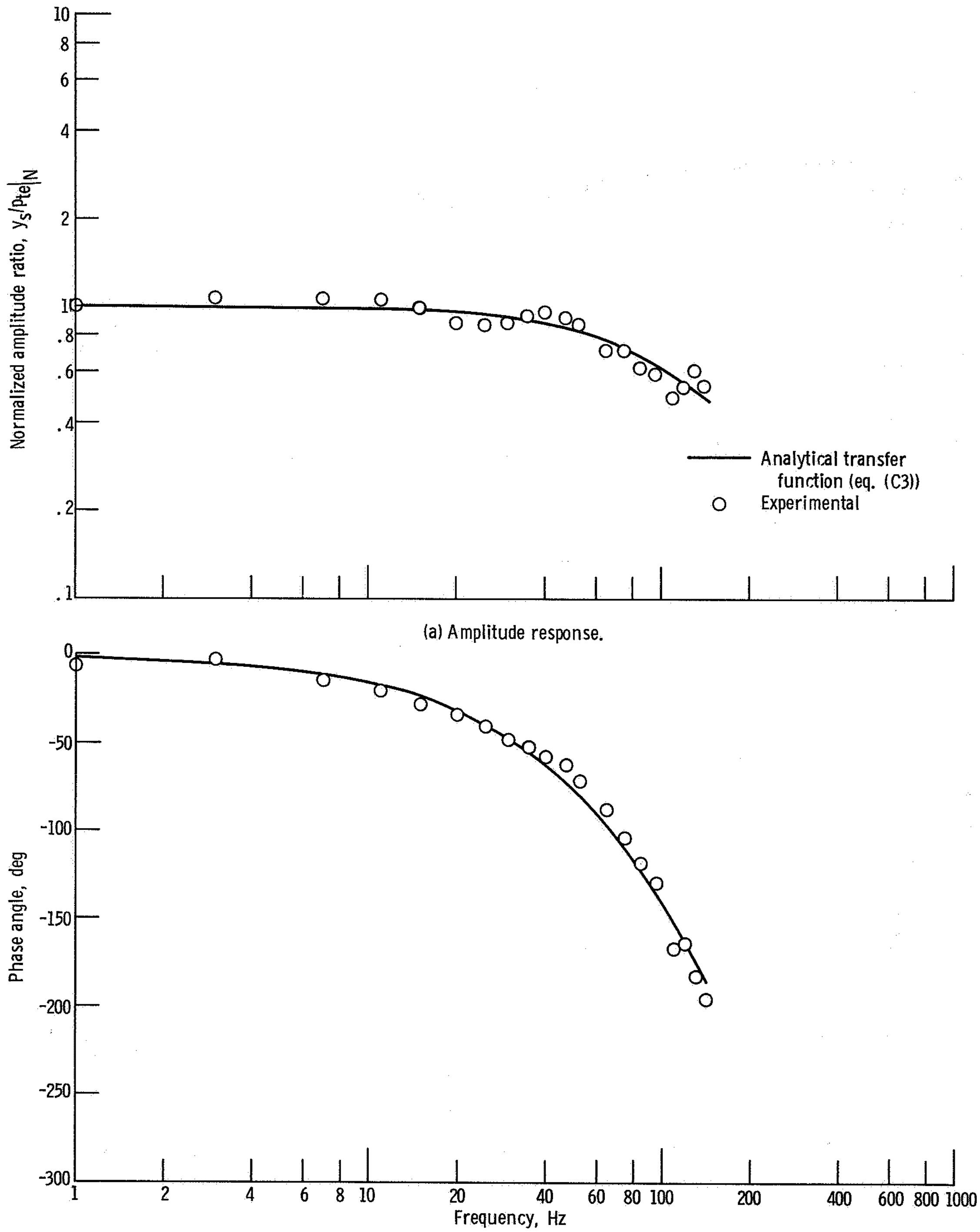

(b) Phase response.

Figure 31. - Comparison of analytical and experimental frequency response performance of shock position to throat exit pressure.

APPENDIX D

DISCRETE CONTROLLER FORMULATION

The inlet discussed in this report is being controlled by an optimal feedback controller described by continuous linear time-invariant differential equations. When expressed in matrix form, these are equations (16) and (17). These equations, when they have been slightly rearranged, are

$$\dot{\hat{x}}(t) = (A - K_e H)\hat{x}(t) + Bu(t) + K_e z(t) \tag{D1}$$

$$u(t) = -K_c \hat{x}(t) \tag{D2}$$

Note that $z(t)$ is the controller input and $u(t)$ the controller output. As discussed in the main text, the optimal controller was implemented with a digital computer as well as an analog computer. The digital version is shown in figure 14. In order to obtain a digital controller algorithm, a discrete-time approximation must be obtained for the continuous-time equations (D1) and (D2). The method used in this report is discussed in the following sections. It should be pointed out that the method used for obtaining the digital control algorithm is not unique, and the technique used is only one of a number of possible approaches.

Discrete Control Algorithm

The solution to the vector-matrix differential equation (D1), at time t_{k+1}, given the state $\hat{x}$ at time t_k is

$$\hat{x}(t_{k+1}) = \varphi_e(t_{k+1} - t_k)\hat{x}(t_k) + \int_{t_k}^{t_{k+1}} \varphi_e(t_{k+1} - \tau)Bu(\tau)\,d\tau + \int_{t_k}^{t_{k+1}} \varphi_e(t_{k+1} - \tau)K_e z(\tau)\,d\tau \tag{D3a}$$

where

$$\varphi_e(t_{k+1} - t_k) = \exp\left[(A - K_e H)(t_{k+1} - t_k)\right]$$

$$\varphi_e(t_{k+1} - \tau) = \exp\left[(A - K_e H)(t_{k+1} - \tau)\right]$$

Let $t_k = kT$ and $t_{k+1} = kT + T$ be successive sampling instants, separated by sample period T. If it is assumed that u and z are constant over $kT \leq t < kT + T$, z and u can be moved out from under the integral signs in equation (D3a) and an expression can be obtained for $\hat{x}(kT + T)$ in terms of $\hat{x}(kT)$, $u(kT)$, and $z(kT)$. Since the digital computer produces a stepwise continuous signal u, u is constant during a sample time ($u(\tau) = u(kT)$, $kT \leq \tau < kT + T$). However, z is not; thus, we must assume that T is small enough so that z is approximately constant during the interval:

$$z(\tau) \cong z(kT) \qquad kT \leq \tau < kT + T$$

Making these substitutions, equation (D3a) becomes

$$\hat{x}(kT + T) = \varphi_e(T)\hat{x}(kT) + \left\{\int_{kT}^{kT+T} \varphi_e[(k + 1)T - \tau]B\, d\tau\right\} u(kT)$$

$$+ \left\{\int_{kT}^{kT+T} \varphi_e[(k + 1)T - \tau]K_e\, d\tau\right\} z(kT) \qquad \text{(D3b)}$$

But since the two integrals in equation (D3b) are independent of k, we can evaluate them for $k = 0$:

$$\hat{x}(kT + T) = \varphi_e(T)\hat{x}(kT) + \left[\int_0^T \varphi_e(T - \tau)B\, d\tau\right] u(kT) + \left[\int_0^T \varphi_e(T - \tau)K_e\, d\tau\right] z(kT) \qquad \text{(D3c)}$$

$$\hat{x}(kT + T) = \varphi_e(T)\hat{x}(kT) + \left[\int_0^T \varphi_e(\tau)B\, d\tau\right] u(kT) + \left[\int_0^T \varphi_e(\tau)K_e\, d\tau\right] z(kT) \qquad \text{(D4)}$$

Since

$$\varphi_e(\tau) = e^{(A-K_eH)\tau}$$

then

$$\frac{d\varphi_e}{d\tau} = (A - K_eH)e^{(A-K_eH)\tau} = (A - K_eH)\varphi_e(\tau)$$

Therefore

$$\varphi_e(\tau)\, d\tau = (A - K_eH)^{-1}\, d\varphi_e \tag{D5}$$

and

$$\int_0^T \varphi_e(\tau)\, d\tau = \int_0^T (A - K_eH)^{-1} d\varphi_e = (A - K_eH)^{-1}\left[e^{(A-K_eH)T} - I\right] \tag{D6}$$

Substituting equation (D6) into equation (D4) yields

$$\hat{x}(kT + T) = \varphi_e(T)\hat{x}(kT) + \left\{(A - K_eH)^{-1}\left[e^{(A-K_eH)T} - I\right]\right\}Bu(kT)$$

$$+ \left\{(A - K_eH)^{-1}\left[e^{(A-K_eH)T} - I\right]\right\}K_ez(kT)$$

Therefore, the discrete controller computer algorithm is defined by equations (D7) and (D8):

$$\hat{x}(kT + T) = \varphi_e(T)\hat{x}(kT) + \Gamma_{ce}u(kT) + \Gamma_m z(kT) \tag{D7}$$

where

$$\varphi_e(T) = e^{(A-K_eH)T}$$

$$\Gamma_{ce} = (A - K_eH)^{-1}\left[e^{(A - K_eH)T} - I\right]B$$

$$\Gamma_m = (A - K_eH)^{-1}\left[e^{(A-K_eH)T} - I\right]K_e$$

and

$$u(kT) = -K_c\hat{x}(kT) \tag{D8}$$

The matrices $\varphi_e(T)$, Γ_{ce}, and Γ_m must be numerically determined for the appropriate sampling time T. Acceptable sampling times are those which result in acceptable stability of the complete system operating with the sampled-data controller.

Stability Considerations

To determine the stability of the closed-loop sampled-data system, the continuous inlet plant described by equations (3) and (5) (repeated here as eqs. (D9a) and (D9b)) can be put in discrete form:

$$\dot{x}(t) = Ax(t) + Bu(t) + Dw(t) \tag{D9a}$$

$$z(t) = Hx(t) + v(t) \tag{D9b}$$

$$x(kT + T) = \varphi_p(T)x(kT) + \Gamma_{cp}u(kT) + \Gamma_d w(kT) \tag{D10a}$$

$$z(kT) = Hx(kT) + v(kT) \tag{D10b}$$

where

$$\varphi_p(T) = e^{AT}$$

$$\Gamma_{cp} = A^{-1}(e^{AT} - I)B$$

$$\Gamma_d = A^{-1}(e^{AT} - I)D$$

Here again, an approximation is made that $w(t)$ and $v(t)$ are assumed to be constant over the sampling interval. Combining equations (D7), (D8), (D10a), and (D10b) results in the following expanded matrix equation, which represents the closed-loop sampled-data system:

$$\begin{bmatrix} \hat{x}(kT + T) \\ \hline x(kT + T) \end{bmatrix} = \left[\begin{array}{c|c} \varphi_e(T) - \Gamma_{ce}K_c & \Gamma_m H \\ \hline -\Gamma_{cp}K_c & \varphi_p(T) \end{array}\right] \begin{bmatrix} \hat{x}(kT) \\ \hline x(kT) \end{bmatrix} + \left[\begin{array}{c|c} \Gamma_m & 0 \\ \hline 0 & \Gamma_d \end{array}\right] \begin{bmatrix} v(kT) \\ \hline w(kT) \end{bmatrix} \tag{D11}$$

Let

$$\varphi_{CL}(T) = \left[\begin{array}{c|c} \varphi_e(T) - \Gamma_{ce}K_c & \Gamma_m H \\ \hline -\Gamma_{cp}K_c & \varphi_p(T) \end{array}\right] \tag{D12}$$

The eigenvalues of $\varphi_{CL}(T)$ determine the stability of the closed-loop system. A sampling time T which results in an eigenvalue with a magnitude greater than one (outside unit circle in the complex plane) is unacceptable. This criteria was used in determining the largest acceptable sampling period.

Matrix Exponential Expansion

Matrix exponentials such as $e^{(A-K_eH)T}$ and e^{AT} can be determined by using a matrix form for the series expansion of e raised to some power. This technique was used in arriving at an acceptable method for determining the matrix coefficients of equation (D7). A brief description of the procedure using a square matrix Z is

$$e^{ZT} = I + ZT + \frac{Z^2T^2}{2!} + \frac{Z^3T^3}{3!} + \ldots \tag{D13}$$

and

$$Z^{-1}(e^{ZT} - I) = Z^{-1}\left(ZT + \frac{Z^2T^2}{2!} + \ldots\right) \tag{D14}$$

If the series is truncated after r terms, equation (D14) becomes

$$Z^{-1}(e^{ZT} - I) = T + \frac{ZT}{2}\left\{T + \frac{ZT}{3}\left[T + \ldots + \frac{ZT}{r-1}\left(T + \frac{ZT^2}{r}\right)\right]\right\} \tag{D15}$$

and equation (D13) becomes

$$e^{ZT} = I + Z\left\{T + \frac{ZT}{2}\left[T + \ldots + \frac{ZT}{r-1}\left(T + \frac{ZT^2}{r}\right)\right]\right\} \tag{D16}$$

The computer subroutine STM whose listing appears at the end of this appendix actually implements equations (D15) and (D16). Enough terms of the expansion are used to ensure that the matrix elements have converged with sufficient accuracy.

Numerical Considerations

The numerical values of the elements of the matrices $\varphi_e(T)$, Γ_{ce}, and Γ_m for a stable sampling time T were found to have a wide spread. The computer on which the control law of equations (D7) and (D8) was programmed used fixed-point machine language. Thus, the numerical spread of the matrix elements created significant scaling problems in programming the controller. Also, the vector-matrix multiplications required to implement equation (D7) (especially $\varphi_e(T)\hat{x}(kT)$) took too much computer time. This was because $\varphi_e(T)$ had few nonzero elements. To alleviate some of these problems, steps were taken to (1) condition the numerical elements to reduce scaling problems, (2) reduce the number of elements in the φ_e matrix, and (3) provide a check on the final results.

It was found that a convenient way to accomplish steps (1) and (2) was to use a block diagonal transformation on φ_e (see ref. 23). This brought the numerical values of φ_e closer together and eliminated many of the multiplications required in executing the computer control law. The block diagonal transformation is now outlined. Let

$$P\hat{q}(kT) = \hat{x}(kT) \tag{D17}$$

$$P\hat{q}(kT + T) = \hat{x}(kT + T) \tag{D18}$$

Substituting equations (D17) and (D18) into equations (D7) and (D8) yields

$$P\hat{q}(kT + T) = \varphi_e(T)P\hat{q}(kT) + \Gamma_{ce}u(kT) + \Gamma_m z(kT)$$

or

$$\hat{q}(kT + T) = P^{-1}\varphi_e(T)P\hat{q}(kT) + P^{-1}\Gamma_{ce}u(kT) + P^{-1}\Gamma_m z(kT) \tag{D19}$$

and

$$u(kT) = -K_c P\hat{q}(kT) \tag{D20}$$

The matrix P is a transformation matrix whose columns are the eigenvectors of $\varphi_e(T)$ if all the eigenvalues are real. If there exists a complex conjugate pair of eigenvalues, the column of P which would correspond to the first half of the eigenvalue pair is set equal to the (vector) sum of the pair of eigenvectors. The column of P which would correspond to the second half of the eigenvalue pair is set equal to the difference of the eigenvector pair. The resulting block diagonal matrix, $P^{-1}\varphi_e(T)P$ has the real eigenvalues of $\varphi_e(T)$ on the diagonal. When complex conjugate pairs are present, the real parts lie on the diagonal with the imaginary parts on the off-diagonals. Where $\varphi_e(T)$ has n^2 nonzero elements, $P^{-1}\varphi_e(T)P$ has n, if all eigenvalues are real, and 3n - 2 if all eigenvalues are complex. This represents a considerable reduction in computer operations required in implementing equation (D19) as compared to equation (D7).

Once the transformation matrix P is determined, the numerical values required by the controller can be determined. The transformation results in a transformed set of estimated states $\hat{q}$. The control output is determined by the transformed control weighting $-K_cP$ on these new estimated states. In determining the control output, each of the transformed state estimates must be calculated. Therefore, the programmer must know what will be extremes or worst case values of these states when operating within the closed-loop experimental system so that he can properly scale the states. To assist the programmer in this area, the system was analyzed analytically to determine worst case magnitudes of the estimated states. This was done by subjecting the closed-loop discrete system to inputs equivalent to the worst case compressor face airflow disturbance anticipated for the experimental program. For the transformed controller, the closed-loop system, as defined by equations (D19) and (D20) together with plant equations (D10a) and (D10b), is

$$\begin{bmatrix} \hat{q}(kT + T) \\ \hline x(kT + T) \end{bmatrix} = \left[\begin{array}{c|c} P^{-1}\varphi_e(T)P - P^{-1}\Gamma_{ce}K_cP & P^{-1}\Gamma_m H \\ \hline -\Gamma_{cp}K_cP & \varphi_p \end{array}\right] \begin{bmatrix} \hat{q}(kT) \\ \hline x(kT) \end{bmatrix} + \left[\begin{array}{c|c} P^{-1}\Gamma_m & 0 \\ \hline 0 & \Gamma_d \end{array}\right] \begin{bmatrix} v(kT) \\ \hline w(kT) \end{bmatrix} \tag{D21}$$

The computer subroutine used to accomplish evaluation of the transient performance of the closed-loop sampled-data inlet system is included in this appendix.

Supporting Computer Programs

In this section is a brief description of the computer routines used in a large central batch processing facility to arrive at an acceptable discrete controller capable of being expeditiously and reliably programmed on the digital control computer system.

Shown in figure 32 is a flow chart of the computer program and its associated subroutines. Once the appropriate constants representing the continuous inlet and its selected estimator/controller are read into the computer, the programs use subroutine STM and a preselected value of sampling time to determine the discrete equivalent of the control and inlet plant. Eigenvalues of the φ_{CL} matrix are then determined for the particular T used. If the eigenvalues are all within the unit circle, then subroutine DIAG is used to effect a coordinate transformation of the state estimator. Finally, the complete closed-loop sampled-data system is exercised through a transient. These transient data show the sizes of the various computer estimated states and feedback con-

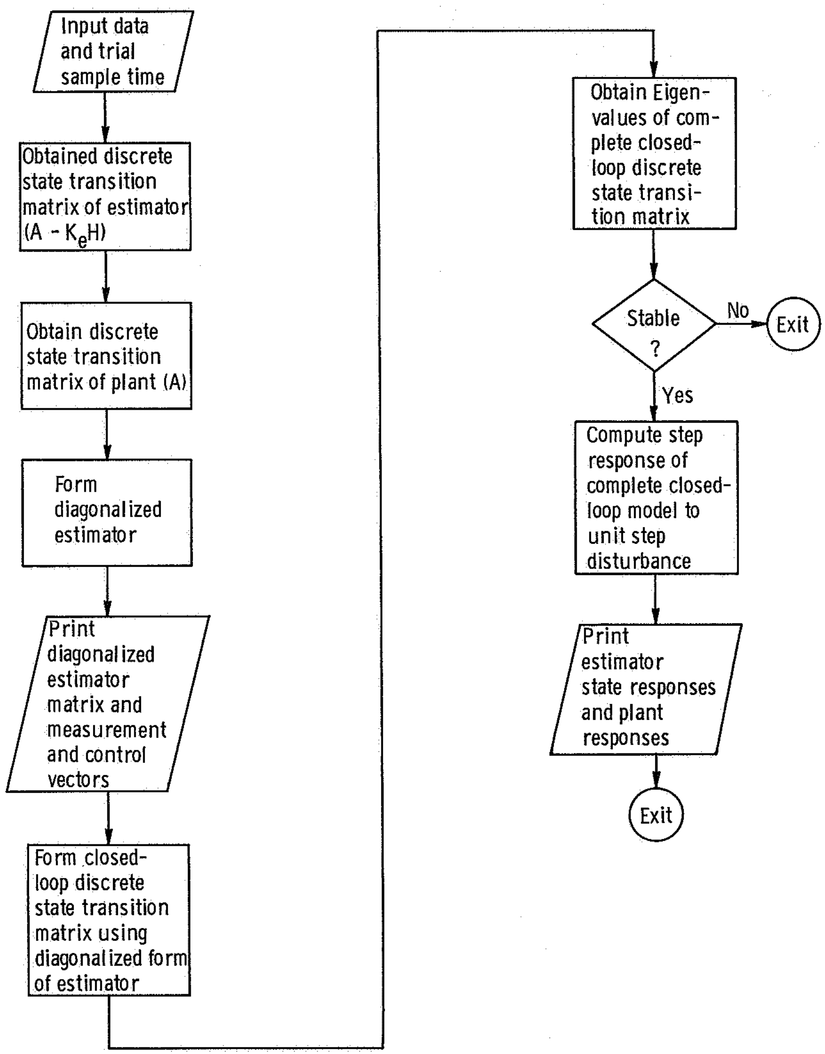

Figure 32. - Flow chart for digital computer program (DIGCON).

trol input and thus are an aid in machine language programming the computer controller.

Listings of the computer programs used in determining the discrete control laws are included in this appendix. Table VI lists the significant equation variables with their corresponding FORTRAN designations. Other information concerning the attached program listing is contained in various comment statements appropriately located throughout the program.

TABLE VI. - CROSS REFERENCE LIST FOR DISCRETE CONTROLLER VARIABLES

Equation variables	FORTRAN variables
φ_e	PHE
Γ_{ce}	GAMU
Γ_m	GAMZ
φ_p	PHP
Γ_{cp}	GAMB
Γ_d	GAMD
K_cP	KCP
$P^{-1}\Gamma_m$	GAMZP
$P^{-1}\Gamma_{ce}$	GAMUP
$P^{-1}\Gamma_{ce}K_cP$	GUKC
$P^{-1}\Gamma_mH$	GZH
$\Gamma_{cp}K_cP$	GBKC

```
$IBFTC DIGCON  LIST
C
C *********************************************************************
C
C      DIGCON DETERMINES A DISCRETE FORM OF A FEEDBACK CONTROL
C      LAW SUITABLE FOR IMPLEMENTATION WITH A DIGITAL COMPUTER.
C      CONTROL WEIGHS ESTIMATES OF THE SYSTEM STATES OBTAINED WITH
C      A KALMAN FILTER.  PREDICTION OF TRANSIENT RESPONSE PERFORMANCE
C      OF CLOSED LOOP SYSTEM TO A STEP DISTURBANCE IS ALSO INCLUDED.
C
C      THE FOLLOWING SUBROUTINES ARE PART OF THE IBM SSP
C         GMPRD - MULTIPLIES TWO GENERAL MATRICES TO FORM
C                 A RESULTANT GENERAL MATRIX.
C         FACTR - PROVIDES FACTURIZATION OF THE INPUT MATRIX
C                 INTO A PRODUCT OF A LOWER TRIANGULAR MATRIX
C                 AND AN UPPER TRIANGULAR MATRIX.
C         HSBG -- REDUCES A REAL MATRIX TO ALMOST TRIANGULAR
C                 (HESSENBURG)FORM.
C         DMINV - INVERTS A DOUBLE PRECISION MATRIX YIELDING
C                 A DOUBLE PRECISION RESULT.
C
C      OTHER SUBROUTINES CALLED BY DIGCON ARE EIGOR, STM, AND DIAG.
C      LISTINGS FOR THESE ARE INCLUDED.
C
C *********************************************************************
C
C      DIMENSION OF VARIABLES
C      A(N,N)
C      B(N,C)
C      H(M,N)
C      KC(C,N)
C      KE(N,M)
C      D(N,C)
C      CC(M,N)
C      SING(N,N)
C      GBKC(N,N)
C      GUKC(N,N)
C      FXT1(N,N)
C      F(N,N)
C      PHP(N,N)
C      GZH(N,N)
C      GAMAT(N,N)
C      GAMB(N,C)
C      GAMD(N,C)
C      KCP(C,N)
C      XS(M,1)
C      P56(M,1)
C      PHBIG(2N,2N)
C      PHFSB(2N,2N)
C      XBIG(2N,1)
C      XNBIG(2N,1)
C      ZBIG(2,1)
C      EX1BIG(2N,1)
C      EX2BIG(2N,1)
C      GAMBIG(2N,2)
C      RR2(2N)
C      RI2(2N)
C      MAG2(2N)
C      PHE(N,N)
```

```
C       GAMU(N,C)
C       GAMZ(N,C)
C       TD(N,N)
C       PHID(N,N)
C       GAMUP(N,C)
C       GAMZP(N,C)
C       AAA(N,N)
C       EIG(N,N,2)
C       CPR(N)
C       CPI(N)
C       RR(N)
C       RI(N)
C       CR(N)
C       CI(N)
C       AH(N,N)
C       LWVD(N)
C       MWVD(N)
C       PPHID(N,N)
C       PHIP(N,N)
C       TT(N,N)
C       EXT16(N,N)
C       PERN(N)
C       IPERN(N)
C       IPER(N)
C       DD(N,N)
C       ED(N,N)
C       Y(N,1)
C       SD(N,1)
C       EX(N,1)
C       QS(N,1)
C       QQQ(N,1)
C       EXT2(2N,2N)
C       PER2N(2N)
C       IPER2N(2N)
C       IPER2(2N)
C       P2S(2N,2N)
C       P2(2N,2N)
C       Q2(2N,1)
C       Z2(2N,1)
C       QS1(2N,1)
C       QP2(2N,1)
C       YD2(2N,1)
        COMMON  / BLDA / A(10,10), B(10,1), H(1,10), KC(1,10), KE(10,1),
       1 D(10,1), CC(1,10)
        DIMENSION  SING(10,10), GBKC(10,10), GUKC(10,10),
       1 EXT1(10,10), F(10,10), PHP(10,10), GZH(10,10), GAMAT(10,10),
       2 GAMB(10,1), GAMD(10,1), KCP(1,10), XS(1,1), P56(1,1),
       3 PHBIG(20,20), PHESB(20,20), XBIG(20,1), XNBIG(20,1), ZBIG(2,1),
       4 EX1BIG(20,1), EX2BIG(20,1), GAMBIG(20,2), RR2(20), RI2(20),
       5 MAG2(20), PHE(10,10), GAMU(10,1), GAMZ(10,1), TD(10,10),
       6 PHID(10,10), GAMUP(10,1), GAMZP(10,1), AAA(10,10), EIG(10,10,2),
       7 CPR(10), CPI(10), RR(10), RI(10), CR(10), CI(10), AH(10,10),
       8 LWVD(10), MWVD(10), PPHID(10,10), PHIP(10,10), TT(10,10),
       9 EXT16(10,10), PERN(10), IPERN(10), IPER(10), DD(10,10),
       A ED(10,10), Y(10,1), SD(10,1), EX(10,1), QS(10,1), QQQ(10,1),
       B EXT2(20,20), PER2N(20), IPER2N(20), IPER2(20), P2S(20,20),
       C P2(20,20), Q2(20,1), Z2(20,1), QS1(20,1), QP2(20,1), YD2(20,1)
        DOUBLE PRECISION  A, B, H, KC, KE, EXT1, TD, F, DT, PHE, GAMU,
       1 GAMZ, PHP, GAMB, GAMD, D, CC, PHID, GAMUP, GAMZP, KCP, TT, PPHID,
       2 PHIP, EX1BIG, EX2BIG, XBIG, ZBIG, XNBIG, GAMBIG, P56, XS, GAMAT,
```

```
    3 PHBIG, GZH, GBKC, GUKC
      REAL   MAG2
      INTEGER   C
      COMMON  / FORM / VFMT(10,6), FMT(6)
C
C
C
      DATA   ((VFMT(I,J),   J = 1,6),   I = 1,10)
     1 / 6H        , 6H        , 6H        , 6H        , 6H  (1P1, 6HE12.4),
     2   6H        , 6H        , 6H        , 6H        , 6H  (1P2, 6HE12.4),
     3   6H        , 6H        , 6H        , 6H        , 6H  (1P3, 6HE12.4),
     4   6H        , 6H        , 6H        , 6H        , 6H  (1P4, 6HE12.4),
     5   6H        , 6H        , 6H        , 6H        , 6H  (1P5, 6HE12.4),
     6   6H        , 6H        , 6H        , 6H        , 6H  (1P6, 6HE12.4),
     7   6H        , 6H        , 6H        , 6H        , 6H  (1P7, 6HE12.4),
     8   6H        , 6H        , 6H        , 6H        , 6H  (1P8, 6HE12.4),
     9   6H        , 6H        , 6H        , 6H        , 6H  (1P9, 6HE12.4),
     A   6H        , 6H        , 6H        , 6H        , 6H (1P10, 6HE12.4)
C
C      IOP IS THE PRINT VARIABLE
C      IF IOP = 0, THERE WILL BE STANDARD OUTPUT
C      IF IOP = 1, THERE WILL BE EXTENDED OUTPUT
C
      IOP = 0
      WRITE (6,35)
      N2 = 20
      N = 10
      M = 1
      C = 1
      DT = .2D0
      KMAXE = 50
      KMAXP = 50
      DO 4   I = 1,N
      DO 3   K = 1,C
      KCP(K,I) = 0.0D0
      GAMU(I,K) = 0.0D0
      GAMZ(I,K) = 0.0D0
      GAMB(I,K) = 0.0D0
    3 GAMD(I,K) = 0.0D0
      DO 4   J = 1,N
      GUKC(I,J) = 0.0D0
      GZH(I,J) = 0.0D0
      GBKC(I,J) = 0.0D0
    4 EXT1(I,J) = 0.0D0
C
C      FORM  (KE * H)
C
      DO 5   K = 1,N
      DO 5   I = 1,N
      DO 5   J = 1,M
    5 EXT1(I,K) = KE(I,J) * H(J,K) + EXT1(I,K)
C
C      FORM  (A - KE * H) ESTIMATOR MATRIX
C
      DO 6   I = 1,N
      DO 6   J = 1,N
    6 F(I,J) = A(I,J) - EXT1(I,J)
      IF (IOP .EQ. 0)   GO TO 329
C
C      PRINT ESTIMATOR MATRIX
```

```
C
      WRITE (6,435)
      DO 501  J = 1,6
 501  FMT(J) = VFMT(N,J)
      WRITE (6,FMT)  ((F(I,J),  J = 1,N),  I = 1,N)
 329  DO 330  I = 1,N
      DO 330  J = 1,N
 330  SING(I,J) = F(I,J)
      CALL FSBG  (N, SING, N)
C
C     DETERMINE EIGENVALUES OF ESTIMATOR  (A - KE * H)
C
      IF (IOP .EQ. 0)  GO TO 328
      WRITE (6,475)
 328  CALL EIGQR  (SING, N, RR, RI, IOP)
C
C     FORM DISCRETE STATE TRANSITION MATRIX FOR ESTIMATOR (A - KE * H)
C
      CALL STM (F, PHE, GAMAT, N, KMAXE, DT, IOP)
C
C     FORM AND PRINT THE INPUT VECTORS FOR THE ESTIMATOR
C
      DO 331  K = 1,C
      DO 331  I = 1,N
      DO 331  J = 1,N
      GAMU(I,K) = GAMAT(I,J) * B(J,K) + GAMU(I,K)
 331  GAMZ(I,K) = GAMAT(I,J) * KE(J,K) + GAMZ(I,K)
      WRITE (6,35)
      WRITE (6,440)
      DO 502  J = 1,6
 502  FMT(J) = VFMT(C,J)
      WRITE (6,FMT)  ((GAMU(I,J),  J = 1,C),  I = 1,N)
      WRITE (6,45)
      WRITE (6,FMT)  ((GAMZ(I,J),  J = 1,C),  I = 1,N)
C
C     FORM DISCRETE STM FOR PLANT (A)
C
      CALL STM (A, PHP, GAMAT, N, KMAXP, DT, IOP)
C
C     FORM AND PRINT THE INPUT VECTORS FOR THE PLANT
C
      DO 332  K = 1,C
      DO 332  I = 1,N
      DO 332  J = 1,N
      GAMB(I,K) = GAMAT(I,J) * B(J,K) + GAMB(I,K)
 332  GAMD(I,K) = GAMAT(I,J) * D(J,K) + GAMD(I,K)
      WRITE (6,35)
      WRITE (6,445)
      DO 503  J = 1,6
 503  FMT(J) = VFMT(C,J)
      WRITE (6,FMT)  ((GAMB(I,J),  J = 1,C),  I = 1,N)
      WRITE (6,45)
      WRITE (6,FMT)  ((GAMD(I,J),  J = 1,C),  I = 1,N)
C
C     DIAGONALIZE THE DISCRETE STM FOR THE ESTIMATOR (A - KE * H)
C
      CALL DIAG (PHE, GAMU, GAMZ, TD, PHID, GAMUP, GAMZP, N, C, N2, AAA,
     1 EIG, CPR, CPI, CR, CI, AH, LWVD, MWVD, RR, RI, PPHID, PHIP, TT,
     2 EXT16, PERN, IPERN, IPER, DD, ED, Y, EXT2, SD, EX, QS, QQQ,
     3 PER2N, IPER2, IPER2N, P2S, P2, Q2, Z2, QS1, QP2, YD2, IOP)
```

```
C
C     PRINT THE TRANSFORMED INPUT VECTORS FOR THE ESTIMATOR
C
      WRITE (6,35)
      WRITE (6,450)
      DO 504  J = 1,6
 504  FMT(J) = VFMT(C,J)
      WRITE (6,FMT)  ((GAMUP(I,J),  J = 1,C),  I = 1,N)
      WRITE (6,45)
      WRITE (6,FMT)  ((GAMZP(I,J),  J = 1,C),  I = 1,N)
C
C     FORM AND PRINT THE TRANSFORMED CONTROL GAINS
C
      DO 319  K = 1,N
      DO 319  I = 1,C
      DO 319  J = 1,N
 319  KCP(I,K) = KC(I,J) * TD(J,K) + KCP(I,K)
      WRITE (6,455)
      WRITE (6,311)
      DO 505  J = 1,6
 505  FMT(J) = VFMT(N,J)
      WRITE (6,FMT)  ((KCP(J,I),  I = 1,N),  J = 1,C)
C
C     FORM AND PRINT THE CLOSED LOOP DISCRETE STM
C
      DO 405  J = 1,N
      DO 405  I = 1,N
      DO 405  K = 1,C
      GUKC(I,J) = GAMUP(I,K) * KCP(K,J) + GUKC(I,J)
      GBKC(I,J) = GAMB(I,K) * KCP(K,J) + GBKC(I,J)
 405  GZH(I,J) = GAMZP(I,K) * H(K,J) + GZH(I,J)
      DO 410  I = 1,N
      DO 410  J = 1,N
      PHBIG(I,J) = PHID(I,J) - GUKC(I,J)
      K = I + N
      PHBIG(K,J) = - GBKC(I,J)
      L = J + N
      PHBIG(I,L) = GZH(I,J)
 410  PHBIG(K,L) = PHP(I,J)
      IF (IOP .EQ. 0)  GO TO 411
      WRITE (6,35)
      WRITE (6,470)
      DO 506  J = 1,6
 506  FMT(J) = VFMT(N,J)
      WRITE (6,FMT)  ((PHBIG(I,J),  J = 1,N),  I = 1,N2)
      K = N + 1
      WRITE (6,FMT)  ((PHBIG(I,J),  J = K,N2),  I = 1,N2)
 411  DO 705  I = 1,N2
      DO 705  J = 1,N2
 705  PHESB(I,J) = PHBIG(I,J)
      CALL HSBG (N2, PHESB, N2)
C
C     FORM AND PRINT EIGENVALUES OF CLOSED LOOP DISCRETE STM
C
      CALL EIGOR (PHESB, N2, RR2, RI2, 0)
      WRITE (6,35)
      WRITE (6,460)
      WRITE (6,1002)
      DO 415  I = 1,N2
      MAG2(I) = SQRT(RR2(I) * RR2(I) + RI2(I) * RI2(I))
```

```
      WRITE (6,1003)  RR2(I), RI2(I), MAG2(I)
  415 CONTINUE
C
C     CHECK STABILITY OF CLOSED LOOP SYSTEM
C     EXIT IF UNSTABLE
C
      DO 321  I = 1,N2
      IF (MAG2(I) .GT. 1.0)  GO TO 13
  321 CONTINUE
      DO 12  LL = 1,C
      DO 322  I = 1,M
      P56(I,1) = 0.0D0
  322 XS(I,1) = 0.0D0
      DO 7  I = 1,N2
      EX1BIG(I,1) = 0.0D0
      EX2BIG(I,1) = 0.0D0
      XBIG(I,1) = 0.0D0
      XNBIG(I,1) = 0.0D0
      DO 7  J = 1,2
    7 GAMBIG(I,J) = 0.0D0
C
C     THIS IS A UNIT STEP
C
      ZBIG(1,1) = 0.0D0
      ZBIG(2,1) = 1.0D0
      DO 8  I = 1,N
      GAMBIG(I,1) = GAMZP(I,LL)
      K = I + N
    8 GAMBIG(K,2) = GAMD(I,LL)
C
C     COMPUTE CLOSED LOOP STEP RESPONSE
C
      WRITE (6,35)
      DO 12  K = 1,300
      DO 9  I = 1,N2
      DO 420  J = 1,N2
  420 EX1BIG(I,1) = PHBIG(I,J) * XBIG(J,1) + EX1BIG(I,1)
      DO 9  J = 1,2
    9 EX2BIG(I,1) = GAMBIG(I,J) * ZBIG(J,1) + EX2BIG(I,1)
      DO 10  I = 1,N2
      XNBIG(I,1) = EX1BIG(I,1) + EX2BIG(I,1)
   10 XBIG(I,1) = XNBIG(I,1)
C
C     PRINT ESTIMATOR STATES
C
      WRITE (6,465)
      DO 507  J = 1,6
  507 FMT(J) = VFMT(N,J)
      WRITE (6,FMT)  (XNBIG(I,1),  I = 1,N)
      DO 425  II = 1,M
      DO 425  J = 1,N
      JJ = J + N
      P56(II,1) = H(II,J) * XNBIG(JJ,1) + P56(II,1)
  425 XS(II,1) = CC(II,J) * XNBIG(JJ,1) + XS(II,1)
C
C     PRINT PLANT OUTPUT RESPONSES
C
      WRITE (6,430)
      WRITE (6,318)  (P56(I,1), XS(I,1),  I = 1,M)
      DO 324  I = 1,M
```

```
      P56(I,1) = 0.0D0
  324 XS(I,1) = 0.0D0
      DO 11  I = 1,N2
      FX1BIG(I,1) = 0.0D0
      FX2BIG(I,1) = 0.0D0
   11 XNBIG(I,1) = 0.0D0
   12 CONTINUE
   35 FORMAT  (1H1)
   45 FORMAT  (1H0)
 1002 FORMAT  (1X / 10X, 10H REAL PART, 10X, 11H IMAG. PART, 10X,
     1 10H MAGNITUDE)
 1003 FORMAT  (8X, E14.7, 6X, E14.7, 6X, E14.7)
  311 FORMAT  (50X, 3HKCP)
  318 FORMAT  (1X, 1P2E20.6)
  430 FORMAT  (14X, 3HP56, 18X, 2HXS)
  435 FORMAT  (1X, 16HESTIMATOR MATRIX)
  440 FORMAT  (1X, 31HINPUT VECTORS FOR THE ESTIMATOR)
  445 FORMAT  (1X, 27HINPUT VECTORS FOR THE PLANT)
  450 FORMAT  (1X, 43HTRANSFORMED INPUT VECTORS FOR THE ESTIMATOR)
  455 FORMAT  (1X, 25HTRANSFORMED CONTROL GAINS)
  460 FORMAT  (1X, 39HEIGENVALUES OF CLOSED LOOP DISCRETE STM)
  465 FORMAT  (1X, 22HESTIMATOR STATE VECTOR)
  470 FORMAT  (1X, 24HCLOSED LOOP DISCRETE STM)
  475 FORMAT  (1X, 24HEIGENVALUES OF ESTIMATOR)
   13 CONTINUE
      STOP
      END
```

```
$IBFTC STM     LIST
      SUBROUTINE  STM (F, PHI, GAMAT, N, KMAX, DT, IOP)
C
C ***************************************************************************
C
C     STM COMPUTES THE STATE TRANSITION MATRIX PHI = EXP( F * DT )
C     USING A NESTED POLYNOMIAL EVALUATION OF THE SERIES REPRESENTATION.
C
C     PHI IS THE OUTPUT S.T.M., GAMAT IS THE OUTPUT MATRIX FOR COM-
C     PUTING THE VECTORS GAMMA, F IS THE INPUT MATRIX, N IS THE SIZE
C     OF THE MATRIX, KMAX IS THE NUMBER OF TERMS IN THE S.T.M. SERIES,
C     AND DT IS THE SAMPLING TIME.
C
C     STM CALLS NO SUBROUTINES.
C
C ***************************************************************************
C
C     DIMENSION OF INPUT VARIABLES
C     F(N,N)
C     DIMENSION OF OUTPUT VARIABLES
C     PHI(N,N)
C     GAMAT(N,N)
      DOUBLE PRECISION  F, PHI, GAMAT, DT, X, Y
      DIMENSION  F(N,N), PHI(N,N), GAMAT(N,N)
      COMMON  / FORM / VFMT(10,6), FMT(6)
C
C
C
C     NN IS THE UNDERFLOW COUNTER
C
      NN = 0
C
C     INITIAL GAMAT IS I * DT
C
      DO 100  I = 1,N
      DO 100  J = 1,N
      GAMAT(I,J) = 0.0D0
      IF (I .EQ. J)  GAMAT(I,J) = DT
  100 CONTINUE
      KMAX1 = KMAX - 1
C
C     SERIES CALCULATION OF GAMAT
C
      DO 400  L = 1,KMAX1
      X = KMAX - L + 1
      X = DT / X
      DO 300  I = 1,N
      DO 300  J = 1,N
      PHI(I,J) = 0.0D0
C
C     PHI IS USED AS TEMPORARY STORAGE FOR THE CALCULATION OF GAMAT
C
      DO 200  K = 1,N
      Y = F(I,K) * GAMAT(K,J) * X
C
C     THE FOLLOWING FOUR STATEMENTS TEST FOR UNDERFLOW CONDITIONS.
C
      IF (Y .EQ. 0.0D0)  GO TO 200
      IF (ABS(Y) .GT. 1.0D-25)  GO TO 200
```

```
      Y = 0.0D0
      NN = NN + 1
  200 PHI(I,J) = PHI(I,J) + Y
      IF (I .EQ. J)  PHI(I,J) = PHI(I,J) + DT
  300 CONTINUE
      DO 400  I = 1,N
      DO 400  J = 1,N
  400 GAMAT(I,J) = PHI(I,J)
C
C     UPON COMPLETION OF THE L DO LOOP, GAMAT CONTAINS THE DESIRED
C     RESULT.  THE REMAINDER OF THE SUBROUTINE COMPUTES PHI BY MULTI-
C     PLYING GAMAT BY F AND ADDING THE IDENTITY MATRIX.
C
      DO 600  I = 1,N
      DO 600  J = 1,N
      PHI(I,J) = 0.0D0
      DO 500  K = 1,N
      Y = F(I,K) * GAMAT(K,J)
      IF (Y .EQ. 0.0D0)  GO TO 500
      IF (ABS(Y) .GT. 1.0D-25)  GO TO 500
      Y = 0.0D0
      NN = NN + 1
  500 PHI(I,J) = PHI(I,J) + Y
      IF (I .EQ. J)  PHI(I,J) = PHI(I,J) + 1.0D0
  600 CONTINUE
      IF (IOP .EQ. 0)  GO TO 800
C
C     PRINT OUTPUT RESULTS
C
      WRITE (6,700)  NN
  700 FORMAT  (1X / 1X, 13HUNDERFLOWS = , I5 // 19X, 3HPHI)
      DO 508  J = 1,6
  508 FMT(J) = VFMT(N,J)
      WRITE (6,FMT)  ((PHI(I,J),  J = 1,N),  I = 1,N)
      WRITE (6,720)
  720 FORMAT  (19X, 5HGAMAT)
      DO 509  J = 1,6
  509 FMT(J) = VFMT(N,J)
      WRITE (6,FMT)  ((GAMAT(I,J),  J = 1,N),  I = 1,N)
  800 CONTINUE
      RETURN
      END
```

```
$IBFTC DIAG     LIST
      SUBROUTINE  DIAG (PHI, GAM1, GAM2, TD, PHID, V1, V2, N, C,N2, AAA,
     1 EIG, CPR, CPI, CR, CI, AH, LWVD, MWVD, RR, RI, PPHID, PHIP, TT,
     2 EXT16, PERN, IPERN, IPER, DD, D, Y, EXT2, SD, X, QS, QQQ, PER2N,
     3 IPER2, IPER2N, P2S, P2, Q2, Z2, QS1, QP2, YD2, IOP)
C
C ***********************************************************************
C
C     DIAG COMPUTES THE BLOCK DIAGONAL FORM (PHID) OF THE MATRIX PHI.
C     IT ALSO FINDS THE TRANSFORMED VERSIONS ( V1 AND V2 ) OF TWO
C     INPUT MATRICES ( GAM1 AND GAM2 RESPECTIVELY ). THE TRANSFORMATION
C     MATRIX TD IS ALSO FOUND.
C
C     DIAG CALLS SUBROUTINES HSBG, EIGVEC, EIGQR, AND DMINV.
C
C ***********************************************************************
C
C     DIMENSION OF INPUT VARIABLES OF LIST
C     PHI(N,N)
C     GAM1(N,C)
C     GAM2(N,C)
C     DIMENSION OF OUTPUT VARIABLES OF LIST
C     TD(N,N)
C     PHID(N,N)
C     V1(N,C)
C     V2(N,C)
C     DIMENSION OF INTERNAL VARIABLES
C     TT(N,N)
C     RR(N)
C     RI(N)
C     CR(N)
C     CI(N)
C     AH(N,N)
C     LWVD(N)
C     MWVD(N)
C     PPHID(N,N)
C     PHIP(N,N)
C     AAA(N,N)
C     CPR(N)
C     CPI(N)
C     EIG(N,N,2)
C     EXT16(N,N)
C     DD(N,N)
C     D(N,N)
C     QQC(N,1)
C     QS(N,1)
C     SD(N,1)
C     Y(N,1)
C     X(N,1)
C     PERN(N)
C     IPERN(N)
C     IPER(N)
C     EXT2(2N,2N)
C     P2S(2N,2N)
C     P2(2N,2N)
C     QS1(2N,1)
C     QP2(2N,1)
C     YD2(2N,1)
C     Q2(2N,1)
```

```
C      Z2(2N,1)
C      PER2N(2N)
C      IPER2N(2N)
C      IPER2(2N)
       INTEGER  C
       DOUBLE PRECISION  PHI, GAM1, GAM2, TD, PHID, V1, V2, PHIP, PPHID,
      1 TT, DET
       DIMENSION  PHI(N,N), GAM1(N,C), GAM2(N,C)
       DIMENSION  TD(N,N), PHID(N,N), V1(N,C), V2(N,C)
       DIMENSION  RR(N), RI(N), CR(N), CI(N), AH(N,N), LWVD(N), MWVD(N),
      1 PPHID(N,N), PHIP(N,N), AAA(N,N), CPR(N), CPI(N), EIG(N,N,2),
      2 EXT16(N,N), DD(N,N), D(N,N), QQQ(N,1), QS(N,1), SD(N,1), Y(N,1),
      3 X(N,1), PERN(N), IPERN(N), IPER(N), EXT2(N2,N2), P2S(N2,N2),
      4 P2(N2,N2), QS1(N2,1), QP2(N2,1), YD2(N2,1), Q2(N2,1), Z2(N2,1),
      5 PER2N(N2), IPER2N(N2), IPER2(N2), TT(N,N)
       COMMON  / FORM /  VFMT(10,6), FMT(6)
C
C
C
       DO 170  I = 1,N
       CPR(I) = 0.0
       CPI(I) = 0.0
       DO 169  K = 1,C
       V1(I,K) = 0.0D0
  169  V2(I,K) = 0.0D0
       DO 170  J = 1,N
       PHID(I,J) = 0.0D0
       AAA(I,J) = PHI(I,J)
  170  AH(I,J) = PHI(I,J)
       CALL HSBG(N, AH, N)
C
C      DETERMINE EIGENVALUES OF PHI MATRIX
C
       IF (IOP .EQ. 0)  GO TO 171
       WRITE (6,438)
  171  CALL EIGQR (AH, N, CR, CI, IOP)
       DO 290  II = 1,N
       CPR(II) = CR(II)
       CPI(II) = CI(II)
  290  CONTINUE
       L = 1
    5  PHID(L,L) = CPR(L)
       L = L + 1
       IF (L .GT. N)  GO TO 430
       IF (CPI(L-1) .EQ. 0.0)  GO TO 5
       PHID(L,L) = CPR(L-1)
       PHID(L-1,L) = - CPI(L-1)
       PHID(L,L-1) = CPI(L-1)
       L = L + 1
       IF (L .GT. N)  GO TO 430
       GO TO 5
C
C      FORM EIGENVECTORS
C
  430  CALL EIGVEC (AAA, CPR, CPI, EIG, N, IOP, N2, EXT16, PERN, IPERN,
      1 IPER, DD, D, QS, QQQ, Y, SD, X, EXT2, PER2N, IPER2N, IPER2, P2S,
      2 P2, QS1, Q2, QP2, YD2, Z2)
       DO 435  I = 1,N
       DO 435  J = 1,N
       TD(I,J) = EIG(I,J,1) + EIG(I,J,2)
```

```
      AH(I,J) = PHID(I,J)
 435  TT(I,J) = TD(I,J)
      IF (IOP .EQ. 0)  GO TO 445
      WRITE (6,436)
      DO 510  J = 1,6
 510  FMT(J) = VFMT(N,J)
      WRITE (6,FMT)  ((PHID(I,J),  J = 1,N),  I = 1,N)
 445  CALL HSBG (N, AH, N)
C
C     DETERMINE EIGENVALUES OF PHID MATRIX
C
      IF (IOP .EQ. 0)  GO TO 446
      WRITE (6,439)
 446  CALL EIGQR (AH, N, RR, RI, IOP)
      CALL DMINV (TT, N, DET, LWVD, MWVD)
      IF (DET .EQ. 0.0D0)  WRITE (6,440)
      DO 450  K = 1,C
      DO 450  I = 1,N
      DO 450  J = 1,N
      V1(I,K) = TT(I,J) * GAM1(J,K) + V1(I,K)
 450  V2(I,K) = TT(I,J) * GAM2(J,K) + V2(I,K)
 436  FORMAT  (18X, 4HPHID)
 437  FORMAT  (1X, 1P10E13.5)
 438  FORMAT  (1X, 25HEIGENVALUES OF PHI MATRIX)
 439  FORMAT  (1X, 26HEIGENVALUES OF PHID MATRIX)
 440  FORMAT  (1X, 62HDET = 0.0 AND BLOCK DIAGONAL TRANSFORMATION MATRIX
     1 IS SINGULAR )
      RETURN
      END
```

```
$IBFTC EIGQR    LIST
      SUBROUTINE  EIGQR (A, M, ROOTR, ROOTI, IPRNT)
C
C ********************************************************************
C
C     EIGQR DETERMINES THE EIGENVALUES OF A REAL MATRIX (A) USING
C     FRANCIS QR ALGORITHM.  MAXIMUM NUMBER OF ITERATIONS IN THE
C     QR PROCESS IS 50.  IF IPRNT IS NOT ZERO, THE EIGENVALUES
C     WILL BE PRINTED OUT.
C
C ********************************************************************
C
C     VARIABLES OF LIST
C     A(M,M)           INPUT MATRIX
C     ROOTR(M,1)       REAL PART OF EIGENVALUES
C     ROOTI(M,1)       IMAGINARY PART OF EIGENVALUES
C
      DIMENSION  A(M,M), ROOTR(M), ROOTI(M), PSI(2), GR(3)
C
C
C
      N = M
      DO 2  I = 1,N
      ROOTR(I) = 0.0
    2 ROOTI(I) = 0.0
      IF (IPRNT)  80,81,80
   80 WRITE (6,104)
   81 ZERO = 0.0
      JJ = 1
  177 XNN = 0.0
      XN2 = 0.0
      AA = 0.0
      B = 0.0
      C = 0.0
      DD = 0.0
      R = 0.0
      SIG = 0.0
      ITER = 0
   17 IF (N- 2)  13,14,12
   13 IF (IPRNT)  82,83,82
   82 WRITE (6,105)  A(1,1)
   83 ROOTR(1) = A(1,1)
      ROOTI(1) = 0.0
    1 RETURN
   14 JJ = - 1
   12 X = (A(N-1,N-1) - A(N,N)) ** 2
      S = 4.0 * A(N,N-1) * A(N-1,N)
      ITER = ITER + 1
      IF (X .EQ. 0.0 .OR. ABS(S / X) .GT. 1.0E-8)  GO TO 15
   16 IF (ABS(A(N-1,N-1)) - ABS(A(N,N)))  32,32,31
   31 F = A(N-1,N-1)
      G = A(N,N)
      GO TO 33
   32 G = A(N-1,N-1)
      F = A(N,N)
   33 E = 0.0
      H = 0.0
      GO TO 24
   15 S = X + S
```

```
      X = A(N-1,N-1) + A(N,N)
      IF (S)  18,19,19
19    SQ = SQRT(S)
      F = 0.0
      H = 0.0
      IF (X)  21,21,22
21    E = (X - SQ) / 2.0
      G = (X + SQ) / 2.0
      GO TO 24
22    G = (X - SQ) / 2.0
      E = (X + SQ) / 2.0
      GO TO 24
18    F = SQRT( - S) / 2.0
      E = X / 2.0
      G = E
      H = - F
24    IF (JJ)  28,70,70
70    D = 1.0E-10 * (ABS(G) + F)
      IF (ABS(A(N-1,N-2)) .GT. D)  GO TO 26
28    IF (IPRNT)  84,85,84
84    WRITE (6,105)  E, F, ITER
      WRITE (6,105)  G, H
85    ROOTR(N) = E
      ROOTI(N) = F
      ROOTR(N-1) = G
      ROOTI(N-1) = H
      N = N - 2
      IF (JJ)  1,177,177
26    IF (ABS(A(N,N-1)) .GT. 1.0E-10 * ABS(A(N,N)))  GO TO 50
29    IF (IPRNT)  86,87,86
86    WRITE (6,105)  A(N,N), ZERO, ITER
87    ROOTR(N) = A(N,N)
      ROOTI(N) = 0.0
      N = N - 1
      GO TO 177
50    IF (ABS(ABS(XNN / A(N,N-1)) - 1.0) - 1.0E-6)  63,63,62
62    IF (ABS(ABS(XN2 / A(N-1,N-2)) - 1.0) - 1.0E-6)  63,63,700
63    VQ = ABS(A(N,N-1)) - ABS(A(N-1,N-2))
      IF (ITER - 15)  53,164,64
164   IF (VQ)  165,165,166
165   R = A(N-1,N-2) ** 2
      SIG = 2.0 * A(N-1,N-2)
      GO TO 60
166   R = A(N,N-1) ** 2
      SIG = 2.0 * A(N,N-1)
      GO TO 60
64    IF (VQ)  67,67,66
66    IF (IPRNT)  88,85,88
88    WRITE (6,107)  A(N-1,N-2)
      GO TO 84
67    IF (IPRNT)  89,87,89
89    WRITE (6,107)  A(N,N-1)
      GO TO 86
700   IF (ITER .GT. 50)  GO TO 63
      IF (ITER .GT. 5)  GO TO 53
701   Z1 = ((E - AA) ** 2 + (F - B) ** 2) / (E * E + F * F)
      Z2 = ((G - C) ** 2 + (H - DD) ** 2) / (G * G + H * H)
      IF (Z1 - .25)  51,51,52
51    IF (Z2 - .25)  53,53,54
53    R = E * G - F * H
```

```
      SIG = E + G
      GO TO 60
 54   R = E * E
      SIG = E + E
      GO TO 60
 52   IF (Z2 - .25)  55,55,601
 55   R = G * G
      SIG = G + G
      GO TO 60
601   R = 0.0
      SIG = 0.0
 60   XNN = A(N,N-1)
      XN2 = A(N-1,N-2)
      N1 = N - 1
      IA = N - 2
      IP = IA
      IF (N - 3)  201,210,260
260   DO 212  J = 3,N1
      J1 = N - J
      IF (ABS(A(J1+1,J1)) - D)  210,210,211
211   DEN = A(J1+1,J1+1) * (A(J1+1,J1+1) - SIG) + A(J1+1,J1+2) *
     1 A(J1+2,J1+1) + R
      IF (DEN)  261,212,261
261   IF (ABS(A(J1+1,J1) * A(J1+2,J1+1) * (ABS(A(J1+1,J1+1) +
     1 A(J1+2,J1+2) - SIG) + ABS(A(J1+3,J1+2))) / DEN) - D)  210,210,212
212   IP = J1
210   DO 214  J = 1,IP
      J1 = IP - J + 1
      IF (ABS(A(J1+1,J1)) - D)  213,213,214
214   IQ = J1
213   DO 200  I = IP,N1
      IF (I - IP)  216,215,216
215   GR(1) = A(IP,IP) * (A(IP,IP) - SIG) + A(IP,IP+1) * A(IP+1,IP) + R
      GR(2) = A(IP+1,IP) * (A(IP,IP) + A(IP+1,IP+1) - SIG)
      GR(3) = A(IP+1,IP) * A(IP+2,IP+1)
      A(IP+2,IP) = 0.0
      GO TO 219
216   GR(1) = A(I,I-1)
      GR(2) = A(I+1,I-1)
      IF (I - IA)  217,217,218
217   GR(3) = A(I+2,I-1)
      GO TO 219
218   GR(3) = 0.0
219   XK = SIGN(SQRT(GR(1) ** 2 + GR(2) ** 2 + GR(3) ** 2), GR(1))
222   IF (XK)  223,224,223
223   AL = GR(1) / XK + 1.0
      PSI(1) = GR(2) / (GR(1) + XK)
      PSI(2) = GR(3) / (GR(1) + XK)
      GO TO 225
224   AL = 2.0
      PSI(1) = 0.0
      PSI(2) = 0.0
225   IF (I - IQ)  226,227,226
226   IF (I - IP)  229,228,229
228   A(I,I-1) = - A(I,I-1)
      GO TO 227
229   A(I,I-1) = - XK
227   DO 230  J = I,N
      IF (I - IA)  231,231,232
231   CR = PSI(2) * A(I+2,J)
```

```
      GO TO 233
232   CR = 0.0
233   ER = AL * (A(I,J) + PSI(1) * A(I+1,J) + CR)
      A(I,J) = A(I,J) - ER
      A(I+1,J) = A(I+1,J) - PSI(1) * ER
      IF (I - IA)  234,234,230
234   A(I+2,J) = A(I+2,J) - PSI(2) * ER
230   CONTINUE
      IF (I - IA)  235,235,236
235   L = I + 2
      GO TO 237
236   L = N
237   DO 240  J = IQ,L
      IF (I - IA)  238,238,239
238   CR = PSI(2) * A(J,I+2)
      GO TO 241
239   CR = 0.0
241   ER = AL * (A(J,I) + PSI(1) * A(J,I+1) + CR)
      A(J,I) = A(J,I) - ER
      A(J,I+1) = A(J,I+1) - PSI(1) * ER
      IF (I - IA)  242,242,240
242   A(J,I+2) = A(J,I+2) - PSI(2) * ER
240   CONTINUE
      IF (I - N + 3)  243,243,200
243   ER = AL * PSI(2) * A(I+3,I+2)
      A(I+3,I) = - ER
      A(I+3,I+1) = - PSI(1) * ER
      A(I+3,I+2) = A(I+3,I+2) - PSI(2) * ER
200   CONTINUE
201   AA = E
      B = F
      C = G
      DD = H
      GO TO 12
104   FORMAT  (////1X, 9HREAL PART, 6X, 14HIMAGINARY PART, 26X,
     1 13HTAKEN AS ZERO, 6X, 4HITER //)
105   FORMAT  (1X, E15.8, 3X, E15.8, 42X, I3)
107   FORMAT  (56X, E13.8)
      END
```

```
$IBFTC EIGVEC  LIST
      SUBROUTINE  EIGVEC (AAA, CPR, CPI, EIG, N, IOP2, N2, EXT16, PERN,
     1 IPERN, IPER, DD, D, QS, QQQ, Y, SD, X, EXT2, PER2N, IPER2N,
     2 IPER2, P2S, P2, QS1, Q2, QP2, YD2, Z2)
C
C *********************************************************************
C
C      EIGVEC DETERMINES THE EIGENVECTORS OF A REAL MATRIX (AAA),
C      GIVEN THE REAL AND IMAGINARY PARTS OF THE EIGENVALUES OF (AAA),
C      CPR AND CPI, RESPECTIVELY.  THE TECHNIQUE USED IS THE VAN NESS
C      INVERSE ITERATION METHOD.  EIGENVECTORS ARE STORED IN A TRIPLE
C      SUBSCRIPTED ARRAY (EIG).  THE REAL PARTS ARE STORED COLUMNWISE
C      IN EIG(I,J,1), AND THE IMAGINARY PARTS IN EIG(I,J,2).  IF IOP2
C      IS NOT ZERO, THE EIGENVECTORS ARE PRINTED OUT.
C
C      EIGVEC CALLS SUBROUTINES FACTR, PERM, AND GMPRD.
C
C *********************************************************************
C
C      DIMENSION OF INPUT VARIABLES OF LIST
C      AAA(N,N)
C      CPR(N)
C      CPI(N)
C      DIMENSION OF OUTPUT VARIABLE OF LIST
C      EIG(N,N,2)
C      DIMENSION OF INTERNAL VARIABLES
C      EXT16(N,N)
C      PERN(N)
C      IPERN(N)
C      IPER(N)
C      DD(N,N)
C      D(N,N)
C      QS(N,1)
C      QQQ(N,1)
C      Y(N,1)
C      SD(N,1)
C      X(N,1)
C      EXT2(2N,2N)
C      P2S(2N,2N)
C      P2(2N,2N)
C      QS1(2N,1)
C      QP2(2N,1)
C      YD2(2N,1)
C      Q2(2N,1)
C      Z2(2N,1)
C      PER2N(2N)
C      IPER2N(2N)
C      IPER2(2N)
C
      DIMENSION  AAA(N,N), CPR(N), CPI(N)
      DIMENSION  EIG(N,N,2)
      DIMENSION  EXT16(N,N), DD(N,N), D(N,N), Y(N,1), SD(N,1),
     1 X(N,1), YD2(N2,1), Z2(N2,1), P2(N2,N2), QS1(N2,1), QP2(N2,1),
     2 PERN(N), IPERN(N), IPER(N), QS(N,1), QQQ(N,1), Q2(N2,1),
     3 EXT2(N2,N2), PER2N(N2), IPER2N(N2), IPER2(N2), P2S(N2,N2)
C
C
C
C
```

```
      L = 1
  310 IF (L .GT. N )  GO TO 430
      IF (CPI(L) .NE. 0.0)  GO TO 360
C     CALCULATE REAL EIGENVECTOR
      DO 315  I = 1,N
      DO 315  J = 1,N
      EXT16(I,J) = AAA(I,J)
      IF (I .EQ. J)  EXT16(I,J) = EXT16(I,J) - CPR(L)
  315 CONTINUE
  316 CALL FACTR (EXT16, PERN, N , N , IER)
      DO 313  I = 1,N
  313 IPERN(I) = PERN(I)
      CALL PERM (IPERN, IPER, N , IERP)
      IF (IERP .EQ. 0)  GO TO 312
      WRITE (6,311)
  311 FORMAT  (1H0, 19HPERN CANNOT BE DONE)
  312 CONTINUE
      IF (IER .NE. 3)  GO TO 319
      WRITE (6,317)
  317 FORMAT  (1H0, 14HFACTR IS WRONG)
      DO 318  I = 1,N
      DO 318  J = 1,N
      IF (EXT16(I,J) .EQ. 0.0)  EXT16(I,J) = .5 / (2.0 ** 35)
  318 CONTINUE
      GO TO 316
  319 DO 320  I = 1,N
      DO 320  J = 1,N
      DD(I,J) = 0.0
      D(I,J) = 0.0
      IF (I .EQ. J)  DD(I,J) = 1.0
  320 CONTINUE
      DO 325  I = 1,N
      IIPER = IPER(I)
      DO 325  J = 1,N
      D(I,J) = DD(IIPER,J)
  325 CONTINUE
      DO 340  I = 1,N
      IF (EXT16(I,I) .NE. 0.0)  GO TO 340
      AMAX = ABS(EXT16(I,1))
      DO 335  J = I,N
      IF (ABS(EXT16(I,J)) .GT. AMAX)  AMAX = ABS(EXT16(I,J))
  335 CONTINUE
      IF (AMAX .EQ. 0.0)  AMAX = 1.0
      EXT16(I,I) = .5 * AMAX / (2.0 ** 35)
  340 CONTINUE
      DO 345  I = 1,N
      QS(I,1) = 1.0
  345 QQQ(I,1) = QS(I,1)
      JQIEND = 0
  346 CALL GMPRD (D, QQQ, Y, N , N , 1)
      SD(1,1) = Y(1,1)
      DO 347  I = 2,N
      SD(I,1) = Y(I,1)
      M = I - 1
      DO 347  J = 1,M
  347 SD(I,1) = SD(I,1) - EXT16(I,J) * SD(J,1)
      X(N ,1) = SD(N ,1) / EXT16(N ,N )
      DO 349  I = 2,N
      J = N - I + 1
      X(J,1) = SD(J,1)
```

```
      M = J + 1
      DO 348  K = M,N
  348 X(J,1) = X(J,1) - X(K,1) * EXT16(J,K)
  349 X(J,1) = X(J,1) / EXT16(J,J)
      IZ = 1
      ZMAX = ABS(X(1,1))
      DO 350  I = 2,N
      ZINT = ABS(X(I,1))
      IF (ZINT .LE. ZMAX)  GO TO 350
      ZMAX = ZINT
      IZ = I
  350 CONTINUE
      ZMAX = 1.0 / X(IZ,1)
      DO 351  I = 1,N
  351 QQQ(I,1) = X(I,1) * ZMAX
      IQ = 0
      DO 355  I = 1,N
      IF (ABS(QQQ(I,1)) .GT. 1.0E-10)  GO TO 352
      QQQ(I,1) = 0.0
      GO TO 353
  352 DIF = ABS(QS(I,1) - QQQ(I,1))
      IF (DIF .GT. .001 * ABS(QQQ(I,1)))  GO TO 355
  353 IQ = IQ + 1
  355 CONTINUE
      IF (IQ .EQ. N )  GO TO 420
      JQIEND = JQIEND + 1
      IF (JQIEND .EQ. 20)  GO TO 358
      DO 356  I = 1,N
  356 QS(I,1) = QQQ(I,1)
      IF (JQIEND .LT. 30)  GO TO 346
      WRITE(6,357) CPR(L)
  357 FORMAT  (1X, 29HSTUCK IN LOOP WHERE CPR(L) = , 1PE14.6,
     128HAND ANSWERS MAY NOT BE RIGHT)
      GO TO 420
  358 DO 359  I = 1,N
      QQQ(I,1) = (QQQ(I,1) + QS(I,1)) / 2.0
  359 QS(I,1) = QQQ(I,1)
      GO TO 346
C     CALCULATE COMPLEX EIGENVECTOR
  360 DO 354  I = 1,N
      DO 354  J = 1,N
  354 EXT16(I,J) = AAA(I,J)
      DO 364  I = 1,N2
      DO 364  J = 1,N2
  364 EXT2(I,J) = 0.0
      DO 365  I = 1,N
      DO 365  J = 1,N
      K = I + N
      JJ = J + N
      EXT2(I,J) = EXT16(I,J)
      EXT2(K,JJ) = EXT16(I,J)
      IF (I .EQ. J)  EXT2(K,J) = - CPI(L)
      IF (I .EQ. J)  EXT2(I,JJ) = CPI(L)
      IF (I .EQ. J)  EXT2(I,J) = EXT16(I,J) - CPR(L)
      IF (I .EQ. J)  EXT2(K,JJ) = EXT16(I,J) - CPR(L)
  365 CONTINUE
  366 CALL FACTR (EXT2, PER2N, N2, N2, IER)
      DO 363  I = 1,N2
  363 IPER2N(I) = PER2N(I)
      CALL PERM (IPER2N, IPER2, N2, IERP)
```

```
      IF (IERP .EQ. 0)  GO TO 362
      WRITE (6,361)
361   FORMAT  (1H0, 20HPER2N CANNOT BE DONE)
362   CONTINUE
      IF (IER .NE. 3)  GO TO 369
      WRITE (6,367)
367   FORMAT  (1H0, 16HFACTR 2 IS WRONG)
      DO 368  I = 1,N2
      DO 368  J = 1,N2
      IF (EXT2(I,J) .EQ. 0.0)  EXT2(I,J) = .5 / (2.0 ** 35)
368   CONTINUE
      GO TO 366
369   DO 370  I = 1,N2
      DO 370  J = 1,N2
      P2S(I,J) = 0.0
      P2(I,J) = 0.0
      IF (I .EQ. J)  P2S(I,J) = 1.0
370   CONTINUE
      DO 375  I = 1,N2
      IIPER = IPER2(I)
      DO 375  J = 1,N2
      P2(I,J) = P2S(IIPER,J)
375   CONTINUE
      DO 390  I = 1,N2
      IF (EXT2(I,I) .NE. 0.0)  GO TO 390
      AMAX = ABS(EXT2(I,1))
      DO 385  J = I,N2
      IF (ABS(EXT2(I,J)) .GT. AMAX)  AMAX = ABS(EXT2(I,J))
385   CONTINUE
      IF (AMAX .EQ. 0.0)  AMAX = 1.0
      EXT2(I,I) = .5 * AMAX / (2.0 ** 35)
390   CONTINUE
      DO 395  I = 1,N2
      QS1(I,1) = 1.0
395   Q2(I,1) = QS1(I,1)
      JQ2END = 0
396   CALL GMPRD (P2, Q2, QP2, N2, N2, 1)
      YD2(1,1) = QP2(1,1)
      DO 397  I = 2,N2
      YD2(I,1) = QP2(I,1)
      M = I - 1
      DO 397  J = 1,M
397   YD2(I,1) = YD2(I,1) - EXT2(I,J) * YD2(J,1)
      Z2(N2,1) = YD2(N2,1) / EXT2(N2,N2)
      DO 399  I = 2,N2
      J = N2 - I + 1
      Z2(J,1) = YD2(J,1)
      M = J + 1
      DO 398  K = M,N2
398   Z2(J,1) = Z2(J,1) - Z2(K,1) * EXT2(J,K)
399   Z2(J,1) = Z2(J,1) / EXT2(J,J)
      IMAX = 1
      J = N + 1
      ZMAX = Z2(1,1) * Z2(1,1) + Z2(J,1) * Z2(J,1)
      DO 400  I = 2,N
      J = I + N
      ZINT = Z2(I,1) * Z2(I,1) + Z2(J,1) * Z2(J,1)
      IF (ZINT .LE. ZMAX)  GO TO 400
      ZMAX = ZINT
      IMAX = I
```

```
 400  CONTINUE
      JMAX = IMAX + N
      ZMAX = SQRT(ZMAX)
      DO 401  I = 1,N
      J = I + N
      Q2(I,1) = (Z2(I,1) / ZMAX) * (Z2(IMAX,1) / ZMAX) + (Z2(J,1) /
     1 ZMAX) * (Z2(JMAX,1) / ZMAX)
      Q2(J,1) = - (Z2(I,1) / ZMAX) * (Z2(JMAX,1) / ZMAX) + (Z2(J,1) /
     1 ZMAX) * (Z2(IMAX,1) / ZMAX)
 401  CONTINUE
      IQ = 0
      DO 405  I = 1,N2
      IF (ABS(Q2(I,1)) .GT. 1.0E-10)  GO TO 402
      Q2(I,1) = 0.0
      GO TO 403
 402  DIF = ABS(QS1(I,1) - Q2(I,1))
      IF (DIF .GT. .001 * ABS(Q2(I,1)))  GO TC 405
 403  IQ = IQ + 1
 405  CONTINUE
      IF (IQ .EQ. N2)  GO TO 410
      JQ2END = JQ2END + 1
      IF (JQ2END .EQ. 20)  GO TO 408
      DO 406  I = 1,N2
 406  QS1(I,1) = Q2(I,1)
      IF (JQ2END .LT. 30)  GO TO 396
      WRITE(6,407) CPR(L), CPI(L)
 407  FORMAT  (1X, 29HSTUCK IN LOOP WHERE CPR(L) = , 1PE14.6,
     1 13HAND CPI(L) = , 1PE14.6,
     228HAND ANSWERS MAY NOT BE RIGHT)
      GO TO 410
 408  DO 409  I = 1,N2
      Q2(I,1) = (Q2(I,1) + QS1(I,1)) / 2.0
 409  QS1(I,1) = Q2(I,1)
      GO TO 396
 410  CONTINUE
C     LOAD EIGENVECTOR MATRIX WITH COMPLEX EIGENVECTOR PAIR
      DO 413  I = 1,N
      J = I + N
      EIG(I,L,1) = Q2(I,1)
      EIG(I,L+1,1) = Q2(I,1)
      EIG(I,L,2) = Q2(J,1)
 413  EIG(I,L+1,2) = - Q2(J,1)
      L = L + 2
      GO TO 310
C     END OF COMPLEX EIGENVECTOR CALCULATICN
C     LOAD EIGENVECTOR MATRIX WITH REAL EIGENVECTOR
 420  DO 425  I = 1,N
      EIG(I,L,1) = QQQ(I,1)
      EIG(I,L,2) = 0.0
 425  CONTINUE
      L = L + 1
      GO TO 310
C     PRINT OUT EIGENVECTOR MATRIX
 430  LL = 1
      LLL = N
      IF (N  .GT. 10)  LLL = 10
      IF (IOP2 .EQ. 0)  GO TO 467
      WRITE (6,440)
 440  FORMAT  (1H1 / 20X, 12HEIGENVECTORS //)
 435  DO 455  I = 1,N
```

```
      WRITE (6,445)  (EIG(I,L,1),  L = LL,LLL)
445   FORMAT  (1X, 1P10E12.4)
      WRITE (6,450)  (EIG(I,L,2),  L = LL,LLL)
450   FORMAT  (5X, 1P10E12.4)
455   CONTINUE
      WRITE (6,465)
465   FORMAT  (1H1)
467   IF (LLL .EQ. N )  GO TO 460
      LL = 11
      LLL = N
      GO TO 435
460   CONTINUE
      RETURN
      END
```

```
$IBFTC PERM     LIST
      SUBROUTINE  PERM(IP1, IP2, N, IER)
C
C ***********************************************************************
C
C     COMPUTE PERMUTATION VECTOR IP2 FOR TRANSPOSITION VECTOR IP1
C
C ***********************************************************************
C
      DIMENSION  IP1(1), IP2(1)
C
C
C
      DO 2   I = 1,N
    2 IP2(I) = I
      DO 6   I = 1,N
      K = IP1(I)
      IF (K - I)   3,6,4
    3 IF (K)   7,7,5
    4 IF (N - K)   7,5,5
    5 J = IP2(I)
      IP2(I) = IP2(K)
      IP2(K) = J
    6 CONTINUE
      IER = 0
      RETURN
C
C     ERROR RETURN - IP1 IS NOT A TRANSPOSITION VECTOR
C
    7 IER = 1
      RETURN
      END
```

REFERENCES

1. Chun, K. S.; and Burr, R. H.: A Control System Concept for an Axisymmetric Supersonic Inlet. J. Aircraft, vol. 6, no. 4, July-Aug. 1969, pp. 306-311.

2. Crosby, Michael J.; Neiner, George H.; and Cole, Gary L.: High Performance Bypass Control for Mixed-Compression Inlets. Paper 68-652, AIAA, June 1968.

3. Barry, F. W.: Development of Atmospheric Gust Criteria for Supersonic Inlet Design. Rep. HSER-5195, Hamilton Standard Division, United Aircraft Corp., Dec. 1968. (Contract NAS 2-4514.)

4. Lehtinen, Bruce; Zeller, John R.; and Geyser, Lucille C.: Optimal Control of Supersonic Inlets to Minimize Unstarts. NASA TN D-6408, 1971.

5. Lehtinen, Bruce; and Zeller, John R.: Application of Quadratic Optimization to Supersonic Inlet Control. IFAC Journal-Automatica, vol. 8, no. 5, Sept. 1972, p. 563.

6. Wasserbauer, Joseph F.: Dynamic Response of a Mach 2.5 Axisymmetric Inlet with Engine or Cold Pipe and Utilizing 60 Percent Supersonic Internal Area Contraction. NASA TN D-5338, 1969.

7. Cole, Gary L.; Neiner, George H.; and Wallhagen, Robert E.: Coupled Supersonic Inlet-Engine Control Using Overboard Bypass Doors and Engine Speed to Control Normal Shock Position. NASA TN D-6019, 1970.

8. Neiner, George H.; Crosby, Michael J.; and Cole, Gary L.: Experimental and Analytical Investigation of Fast Normal Shock Position Controls for a Mach 2.5 Mixed-Compression Inlet. NASA TN D-6382, 1971.

9. Lin, Y. K.: Probabilistic Theory of Structural Dynamics. McGraw-Hill Book Co., Inc., 1967, pp. 293-297.

10. Skelton, Grant B.: Launch Booster Gust Alleviation. Paper 66-969, AIAA, Nov. 1966.

11. Bryson, Arthur E., Jr.; and Ho, Yu-Chi: Applied Optimal Control. Blaisdell Pub. Co., 1969, pp. 414-447.

12. Cole, Gary L.; Neiner, George H.; and Crosby, Michael J.: Design and Performance of a Digital Electronic Normal Shock Position Sensor for Mixed-Compression Inlets. NASA TN D-5606, 1969.

13. Dustin, Miles O.; Cole, Gary L.; and Wallhagen, Robert E.: Determination of Normal-Shock Position in a Mixed-Compression Supersonic Inlet. NASA TM X-2397, 1971.

14. Neiner, George H.: Servosystem Design of a High-Response Slotted-Plate Overboard Bypass Valve for a Supersonic Inlet. NASA TN D-6081, 1970.

15. Schultz, Donald G.; and Melsa, James L.: State Functions and Linear Control Systems. McGraw-Hill Book Co., Inc., 1967.

16. Neiner, George H.; Cole, Gary L.; and Arpasi, Dale J.: Digital-Computer Normal-Shock-Position and Restart Control of a Mach 2.5 Axisymmetric Mixed-Compression Inlet. NASA TN D-6880, 1972.

17. Arpasi, Dale J.; Zeller, John R.; and Batterton, Peter G.: A General Purpose Digital System for On-Line Control of Airbreathing Propulsion Systems. NASA TM X-2168, 1971.

18. Kuo, Benjamin C.: Analysis and Synthesis of Sampled-Data Control Systems. Prentice-Hall, Inc., 1963.

19. Tou, Julius T.: Digital and Sampled-Data Control Systems. McGraw-Hill Book Co., Inc., 1959.

20. Dorf, Richard C.: Time-Domain Analysis and Design of Control Systems. Addison-Wesley Publ. Co., Inc., 1965.

21. Cubbison, Robert W.; Meleason, Edward T.; and Johnson, David F.: Effect of Porous Bleed in a High-Performance Axisymmetric, Mixed-Compression Inlet at Mach 2.50. NASA TM X-1692, 1968.

22. Cubbison, Robert W.; Meleason, Edward T.; and Johnson, David F.: Performance Characteristics from Mach 2.58 to 1.98 of an Axisymmetric Mixed-Compression Inlet System with 60-Percent Internal Contraction. NASA TM X-1739, 1969.

23. Ogata, Katsuhiko: State Space Analysis of Control Systems. Prentice-Hall, Inc., 1965.

NASA-Langley, 1973 —— 28 E-7173